Xavier Mongiardim Pinto de Mascarenhas

Licenciado em Ciências de Engenharia de Micro e Nanotecnologia

MoS_2 nanosheets as interlayer in Li-S batteries

Dissertação para obtenção do Grau de Mestre em Engenharia de Micro e Nanotecnologias

Orientador: Prof. Dr. Luís Miguel Nunes Pereira, Associate Professor, FCT UNL

Co-Orientador: Prof. Dra Silvia Bodoardo, Associate Professor, Politecnico Di Torino, Italy

Júri:

Presidente: Prof. Dr.

Arguente: Prof. Dr.

Vogal: Prof. Dr.

FACULDADE DE CIÊNCIAS E TECNOLOGIA
UNIVERSIDADE NOVA DE LISBOA

MoS2 Nanosheets as Interlayer in Li-S Batteries

Acknowledgement

Em primeiro lugar, desejo agradecer à Professora Dra. Elvira Fortunato e ao Professor Dr. Rodrigo Martins pela oportunidade concedida ao criar o Mestrado Integrado em Engenharia de Micro e Nanotecnologias e pelas condições disponibilizadas no CENIMAT|i3N e no CEMOP.

Gostaria de agradecer ao meu orientador, Dr. Luís Pereira e à minha co-orientadora Dra. Silvia Bodoardo pela criação de um tema bastante interessante e desafiante, assim como uma orientação atenta e presente durante toda a dissertação, mesmo em alturas mais complicadas ou atarefadas.

Gostaria de agradecer ao meus colegas de laboratório e amigos Paul Grey e Inês Cunha pela paciência e vontade de ajudar e pela harmonia criada em laboratório.

Gostaria também de agradecer a incansável ajuda por parte de Danile Versaci, por me apresentar os cantos do laboratório e me auxiliar em todas as dúvidas que foram geradas durante o meu periodo em Turim.

Gostaria de agradecer à Maria João Oliveira, Dra. Joana Vaz Pinto, à Sonia Pereira e à Dra. Daniela Gomes pelo tempo dispendido na caracterização das minhas amostras e por fazê-lo sempre com um sorriso.

Um agradecimento também à professora Susete Fernandes por me permitir usar a centrifugadora e ao Ricardo pela disponibilidade e ajuda.

Aos dois irmãos que fiz durante este curso – Pedro Centeno e Gonçalo Narciso – pelos momentos passados a trabalhar e os que não foram tanto a trabalhar.

A todos os meus amigos – Simão, Rui, Sara, Rita, Beatriz, Francisca e António – por me motivarem a ser uma pessoa melhor.

Um agradecimento aos meus pais, que tiveram de me sustentar até à data e que me deram bons valores para a vida.

Queria também dirigir o agradecimento aos meus primos que adoro e me porporcionam momentos de família inesquecíveis – Maria Janeiro, José Maria Monteiro, Luis Palmares, Manuel Morais e Isabel Morais.

Um agradecimento às minhas amigas – Laura Serrano e Catarina Rijo – por me conseguirem sempre fazer rir pelo seu sentido de humor.

Ao Emanuel e à sua família pelo seu espírito de acolhimento e outras bebidas espirituosas.

Finalmente, às mais recentes aquisições de amizade, Maria Francisca, Inês e Tânia por transmitirem uma enorme algeria à sua volta.

Abstract

This work has investigated the use of MoS_2 nanosheets acting as an interlayer to effectively block polysulfide shuttling (movement from cathode to the anode) in Li-S batteries.

In the first part of the work we exfoliated bulk MoS_2 into a few layered MoS_2 flakes, resulting in increased surface area and improved electric properties, to achieve a better interlayer performance by effectively trapping polysulfide (PS) in the cathode. This was done through solvothermal lithium intercalation followed by water sonication, creating a reaction between water and intercalated lithium to promote exfoliation.

In the second part was explored the electrochemical characterization of distinct Li-S test cells (each with different interlayers), and compared to a standardized Li-S test cell. The afore mentioned interlayers were spread either on to the cathode or the separator. Furthermore, carbon black, bulk and exfoliated MoS_2, were compared as active materials of the interlayers.

Bulk MoS_2 exfoliation into thinner flake, resulted in a size reduction up to 56 times and a decrease in the number of layers. The results of optical spectroscopy suggest effects of quantum confinement. Furthermore, with XRD, was analytically demonstrated successful intercalation and exfoliation. Then, through Raman and SEM analysis demonstrated evidence of thinner MoS_2 structures.

On another hand, exfoliated MoS_2 was spread on a sulfur cathode creating the interlayer that successfully trapped polysulfides. This was showed through a 4 percentage points increase in sulfur utilization for the first cycle, and an improvement of sulfur loss by cycle of 0.02% retaining a good 99.4% coulombic efficiency. In addition a ΔE decreased of 45%, a result of improved battery kinetics. Nonetheless a simple carbon black DL interlayer was also made using a different solvent. However was observed a increase of sulfur utilization by 9% in the first cycle and the same degradation of sulfur per cycle as the standard battery with an impressive CE of 99.7%.

Resumo

Este trabalho investigou o uso de nanopartículas de MoS_2 a atuar como intercamada que bloqueia efetivamente o movimento de polissulfetos do cátodo para o ânodo, em baterias Li-S. Na primeira parte do trabalho, foi esfoliádo MoS_2 para reduzir a espessura do material, de maneira a aumentar a área de superfície e obter propriedades elétricas aprimoradas, para melhorar o desempenho da intercamada, ao bloquear efetivamente o movimento de polissulfetos para o ânodo. Isto foi feito através da intercalação solvotérmica de lítio seguido de uma sonicação em água, para criar uma reação entre a água e o lítio intercalado e promover a esfoliação.

Na segunda parte, foi explorada a caracterização eletroquímica de distintas células de teste Li-S (cada uma com uma intercamada diferente) e comparadas a uma célula de teste Li-S padronizada. As interlcamadas mencionadas acima, foram espalhadas no catodo, ou no separador. Além disso, CB, MoS_2 em bulk e esfoliado, foram comparados como materiais ativos das intercamadas.

A esfoliação de MoS_2 resultou numa redução de tamanho lateral até 56 vezes e uma diminuição no número de camadas (flocos mais finos). Os resultados da espectroscopia óptica sugerem efeitos do confinamento quântico, observados por uma alteração do hiato energético do material. Além disso, com DRX, foi demonstrado analiticamente uma intercalação e esfoliação bem-sucedidas. Posteriormente, através de uma análise de Raman e SEM, foi observado uma estrutura de MoS_2 mais fina.

Por outro lado, o MoS_2 esfoliado foi espalhado num cátodo de enxofre, para criar a intercamada que captura os polissulfetos. Isto foi demonstrado através de um aumento de 4 pontos percentuais da utilização de enxofre no primeiro ciclo, e um decréscimo na perda de enxofre por cada ciclo de 0.02%, também manteve uma elevada eficiência coulômbica de 99.4%. Além disso, o valor de ΔE diminuiu em 45%, que se traduz em reacções cinéticas mais rápidas na célula de teste. No entanto, também foi testada uma simples intercamada de CB com o uso de um solvente diferente. Foi observado um aumento na utilização de enxofre de 9% no primeiro ciclo e a mesma degradação de enxofre por ciclo que a bateria padrão, com uma eficiência coulombica impressionante de 99.7%.

Abreviations

PS - polysulfides

Li - lithium

S - sulfur

LiTFSI - Lithium bis(trifluoromethanesulfonyl)imide

PVDF - polyvinyldene flouride

NMP - N-metil-2-pirrolidona

CB - carbon black

MoS_2 - molybdenum disulfide

TMD - transition metal dichalcogen

LiOH - lithium hydroxide

PSI - pounds per square inch

H_2 - hydrogen

SEM - scanning electron microscope

XRD - X-ray diffractogram

DLS – dynamic light scattering

FWHM – full width at half measure

AC – alternative current

EIS – electrochemical impedance spectroscopy

CE – coulombic efficiency

Rs – solution resistance

EOD – end of discharge

ΔE – potential polarization

Table of contents

List of figures

Motivation and Objectives

Batteries are the heart of portable electronic equipment, often used in today's society, providing energy to power portable computers, cellphones, electric vehicles and more.

The battery's components and production costs affect's the final price of the product so pursuing research in cheaper, less toxic materials impacts the stock markets for this type of products and therefore the consumer.

Global warming and the Paris agreement created the need for alternative energies to fossil fuels, such can be solar, wind or hydric among others. The major issues with this energy sources are related with energy lost, therefore harnessing this lost energy in high energy density batteries, could improve the performance of these cleaner alternative sources [1].

In the 1990's Sony commercialized the first Li ion batteries, being one of the most important in the market. These batteries are mostly based on lithium compound cathodes, that rely on lithium insertion to harness energy, which possess a discharge capacity around 180mA h g^{-1} and an energy density between 500 and 600 W h kg^{-1}.

Lithium-sulfur technology, promises a theoretical energy density of 2600W h kg^{-1}, almost five times higher than the conventional batteries, and have a theoretical discharge capacity of 1672 mA h g^{-1}, which is almost 10 times higher than the ones based on insertion cathodes [1], [2]. Another big advantage is that sulfur is very abundant on earth and provides for a wide range of operating temperatures.

The biggest existing problem in this type of batteries is polysulfide shuttle, in which soluble polysulfides formed at the cathode travel to the anode, and form non-soluble polysulfides in a parasitic like reaction that doesn't contribute to battery capacity, resulting in loss of capacity, slow kinetics and shorter the lifespan of the battery.

The solution we propose for this problem is creating an interlayer between the anode and the cathode, based on exfoliated molybdenum disulfide monolayers, which trap polysulfides in the cathode, therefore improving battery efficiency.

Molybdenum disulfide has been studied as an interlayer for Li-S batteries, due to the capability to physically and to chemically adsorb the PS. Moreover, when exfoliated into monolayer, MoS_2 presents improved electric properties, a higher surface area, enhanced selectivity and sensitivity, which are features highly attractive for improving the block of PS.

1 Introduction

1.1 Lithium-Sulfur Batteries

Lithium ion batteries (LIBs) are the commercial dominant battery technology , namely those relying on insertion-compound cathode materials[3]. However the limited insertion capability of these compounds limits the maximum energy density, with a maximum around 250 mA h/g [4], [5].

New lithium-sulfur (Li-S) battery technology promises much higher energy storage capacity compared to common commercial batteries. Sulfur is a material that undergoes through a conversion reaction to form polysulfides (PS) [6], allowing for larger accommodation of ions and electrons (two per sulfur atom) [7], conferring sulfur cathode batteries an incredible high theoretical capacity of 1672 mA h/g [8]–[10]. In addition, sulfur allows for a wide range of operation temperature, being non-toxic and a very abundant (thus low-cost) element [11], [12].

On the other hand, lithium is lightest alkali metal, having also the smallest atomic radius among these elements, being highly reactive. It is a very exciting material to be used as anode since it has a theoretical capacity of 3861 mA h/g and possesses the most negative potential among known electrode materials[11], [13].

Sulfur has a crown like structure called S8 ring comprised of 8 sulfur atoms, in this state sulfur is charged. During discharge lithium ions and electrons are generated at the anode and lithium ions move to the cathode through the electrolyte while electrons move through the outside circuit to the cathode, generating an electrical current eq 1.1 [4],[7].

When lithium ions and electrons reach the cathode sulfur reduction occurs, the S8 ring opens to form high order PS Li_2S_x ($4>x\leq8$) eq 1.2, also known as long chain soluble PS, responsible for 25% of discharge capacity value. As discharge keeps going high order PS get further reduced to low order PS [5], [12], [14] which are responsible for the remaining 75% of galvanometric capacity [15], (Figure 1.1). During charge the reverse reactions occurs, where charge is given to the battery restoring electrons to the cathode to convert low order PS back to high order PS and sulfur.

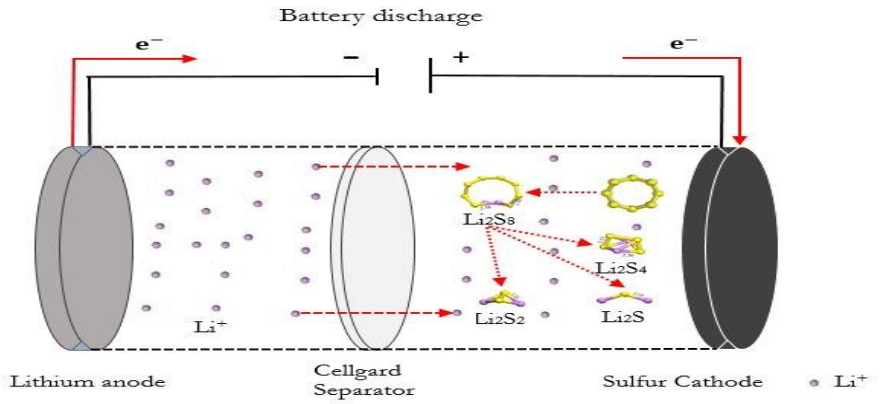

Figure 1-1 Representation of discharge of a regular Li-S battery

$$2Li \rightleftharpoons 2e^- + 2Li^+ \quad \text{(Anodic reaction, Oxidation)} \quad (1.1)$$

$$S + 2Li^+ + 2e^- \rightleftharpoons Li_2S \quad \text{(Cathodic reaction, Reduction)} \quad (1.2)$$

1.1.1 Li-S batteries problems

The main problem in sulfur batteries is when long chain PS generated at the cathode, which happen to be highly soluble in common liquid electrolytes[4], migrate to the anode due to concentration gradient of PS and react with lithium, forming lower order insoluble PS in a parasitic reaction that has no electrochemical contribution to the battery capacity.

The low order PS diffuse back to the cathode and convert back to higher order PS and the process repeats itself indefinitely. Intense PS shuttle can take the battery to an infinite recharge and results in poor charge efficiency (Figure 1.2)[14].

Sulfur high order PS, continuo to slowly dissolve in the electrolyte even in resting state, resulting in a decrease of open circuit voltage and discharge capacity also known has self-discharge [6][5].

Another related issue with shuttling is that sulfur and PS behave has insulator creating passivation of the anode. [16], [17].

On the other hand, and because we are dealing with a lithium anode battery, during charge this metal is deposited on the negative electrode's surface with the risk of forming lithium dendrites leaving only the part in contact with the electrode surface available for electrochemical reaction. [12]

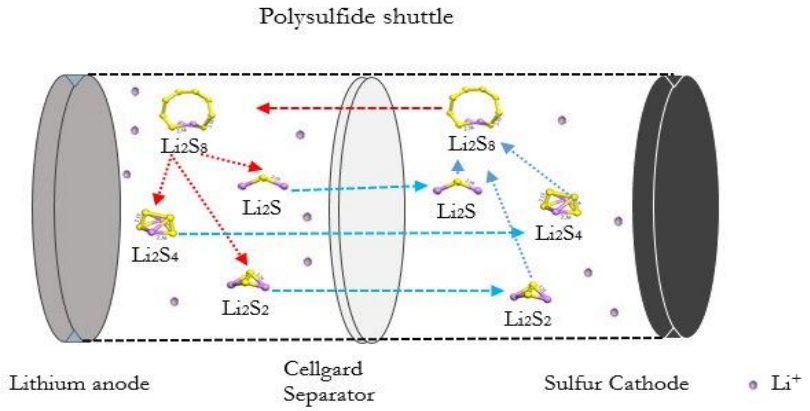

Figure 1-2 Representation of polysulfide shuttle effect inside a regular Li-S battery

1.1.2 State of the art solutions

To solve the problems associated with Li-S batteries there are two main approaches both restricting the PS shuttling, the first one used in this work is to trap the PS with in a porous conductive matrix in the cathode and the second approach is to prevent the PS from dissolving into the electrolyte using a solid state electrolyte.

The matrix can be carbonaceous materials (reduced graphene oxide, carbon black, carbon nanotubes), conductive polymers (PANI, PEDOT:PSS, PEO, PPy), metal oxides (TiO_2) and metal disulfides (MoS_2,WS_2) that block the polysulfides in the cathode region, preventing degradation of the battery, either by physical blocking, electrostatic repulsion in the case of conductive polymers, or chemical absorbance like the case of metal disulfides [4][18], [19][20][21].

Research on MoS_2 nanosheets achieved by solvothermal synthesis and applied on Celgard via vacuum filtration shown results of 1516 mA h/g initial discharge capacity at C/5 and a discharge capacity of 880 mA h/g after 100 cycles with a CE of 98.7% revealing very efficient PS trapping [22]. Another approach already developed was the incorporation of MoS_2 nanosheets into vertically aligned hollow carbon microtube which reached an initial discharge capacity of 750 mA h/g at 1C and after 300 cycles the discharge capacity was at 480 mA h/g revealing an impressive capacity fading per cycle of 0.15% [23]. Conductive Polymers like C-PANI revealed an initial discharge capacity of 1101 mA h/g at C/5 and after 100 cycles a discharge capacity of 835 mA h/g with 90 % CE [24]. Moreover, solid state technology was studied with flexible PVDF gel polymers reaching 936 mA h/g initial discharge capacity at C/10 and after 80 cycles a discharge capacity of 610 mA h/g [25].

1.2 Battery architecture

A standard Li-S battery is comprised of two electrodes (sulfur cathode, a lithium anode) that compress closer together the components inside the battery with the purpose of creating a better connection. In between there is a separator soaked in an ion conductive electrolyte [4], [5], [9], [22], [26]. The separator is a permeable microporous membrane used to keep the two electrodes apart to prevent short circuits between anode and cathode, serving as a good ionic charge transport, and at the same time acts as an electron isolator[22].

Lithium ions move through the electrolyte while electrons move through the external electrical circuit to the positive electrode generating an electrical current (see figure 1.2) [4].

The electrolyte used, LiTFSI ($LiC_2F_6NO_4S_2$), replaces commonly used organic solutions that happen to be flammable and volatile. Ionic liquids add unique properties such has wide range of temperature operation, non-volatility, non-flammability and sufficiently high conductivity for battery applications, which make LiTFSI an appropriate media for Li^+ ion transport. The main problem is that PS are soluble also in this ionic liquid electrolyte, and this PS concentration increases electrolyte viscosity leading to decrease in the ionic conductivity and slower battery kinetic reactions [27], [28]

1.2.1 Cathode

The Cathode active material in Li-S batteries is sulfur, that is connected together by a carbon black porous matrix, linked by a PVDF binder dissolved in NMP solution [4], [29].

Sulfur in Li-S batteries, suffers from a volume change of 80% caused by difference in sulfur's density from (2.03g/cm^3) to complete lithiation discharge product Li_2S (1.66 g/cm^3) that causes structural collapse and poor electrochemical stability [22]. In order to prevent this issue, carbon black is used as a matrix to imprison sulfur inside, forming carbon black clusters with a homogeneous sulfur distribution in it's matrix, providing excellent contact are between sulfur and conductive carbon. Carbon black also acts as an adsorbing agent, preventing PS from leaving the structure [4], at the cost of losing some energy density since CB does not contribute to battery capacity [17]. For this reason, usually amount of CB is kept as low as possible. However this method still has room for improving since Coulombic efficiencies generally drop 75-85% after an average of 200-300 cycles in most cases [17], therefore introduction of a new interlayer between the electrodes that helps to block PS and increase sulfur loading is of great interest [17].

The binder plays an important role has a dispersion agent, linking the electrode materials together and connect them to the current collectors, also cooperating in cycle stability. PolyVinyldene Flouride (PVDF) is the most frequently used providing favorable thermal and chemical stability between electric contact and deposited electrode materials, is soluble in N-methil-2-pyrolidone (NMP), used to control viscosity of PVDF [30].

1.2.2 MoS_2 interlayer function

There are already few approaches in order to resolve problems related with PS shuttling and self-discharge. One of them was mentioned before, that consists in the addition of an overlayer able to absorve PS and physically trap them inside the cathode (see figure 1.3). This is the method that will be studied in standard battery cells during this dissertation. Another method includes changing to a solid electrolyte, creating a solid state battery so PS don't dissolve into the electrolyte [4]. Both of these methods prevent PS shuttling consequently increasing charge capacity and in long term the battery lifetime. Therefore, new materials that possess these capabilities are of great interest for the development of interlayers in Li-S batteries.

Currently most interlayer separators are graphene based [4] which bear great physical blocking of PS, but still not effective enough in preserving long life time for this types of batteries [31]. The morphology of re-oxidized sulfur is affected by the involving conductive carbon and not by original sulfur morphology, affecting sulfur utilization in this type of batteries [4].

Metal sulfides which can chemically bond to PS, like 2D TMDs such as MoS_2, are introduced to create an interlayer between the cathode and the separator with intent to improve PS blocking and enhance electrochemical performance. Exfoliated 2D MoS_2 layers with great flexibility, provide a large active conductive surface area ideal for a successful PS trapping. Moreover it can be easily deposited either on to the separator or directly on the cathode, creating a second layer of protection after CB matrix, while maintaining great ion transportation which helps to improve battery life cycle and efficiency which are the two main issues with Li-S batteries. [17], [26]

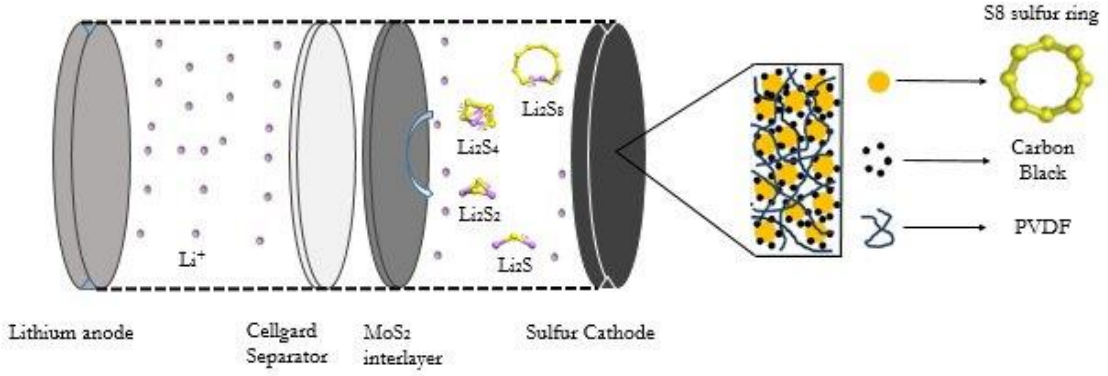

Figure 1-3 Representation of MoS2 interlayer function in a standard Li-S battery

1.3 Molybdenum disulfide

Transition Metal Dichalcogenides are represented by a generalized formula of MX_2, where M is a transition metal from periodic table group´s (4-10) and X is a chalcogen found in the sixteen group of the periodic table [32], [33]. In MoS_2 a layer of molybdenum atom´s with oxidation state +4 is covalently bonded to two sulfur atoms, each with an oxidation state of -2, to form a sandwiched like structure that corresponds to a sheet of with a thickness of 6.7Å [34], [35].

The flat surface of the nanosheet is known as the basal plane and side view of the nanosheet called the edge plane [36].

In its natural bulk form MoS_2 has a 3D structure formed by layers of sheets piled together and connected by Van der Walls bonds with a interlayer spacing of 6.5Å between each sheet [33], [37].

The 2H (Hexagonal) structure, also known has trigonal prismatic phase is the thermodynamically stable phase of MoS_2. This crystal structure coordinated around a molybdenum atom bonded to two symmetric tetrahedrons in +Z and –Z directions to six sulfur atoms and this structure can be seen along the basal plane with hexagonal symmetry (Figure 1.4) [38].

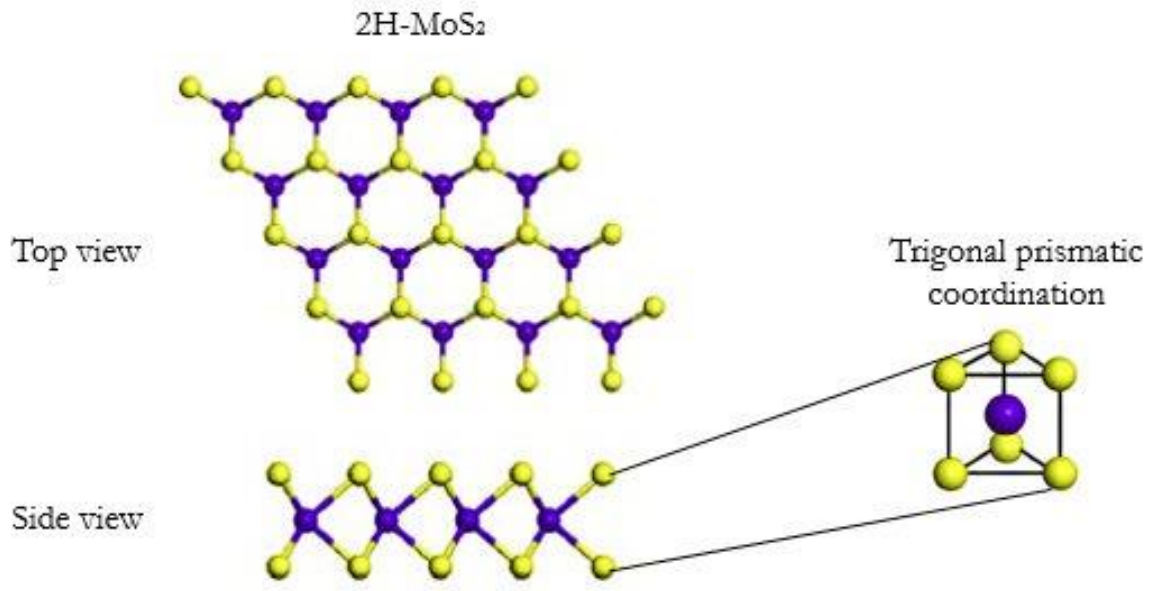

Figure 1-4 Representation of MoS_2 2H structure in basal plane view on the left and the trigonal prismatic coordination on the right image adapted from ref [34]

1.3.1 MoS_2 nanosheets

There two main ways to produce nanosheets are top down approaches where we start from MoS_2 3D bulk structure and exfoliate in order to produce scaled down 2D structures, or bottom up approaches involving the formation of MoS_2 nanosheets through intermediate products at high temperatures [39], like Chemical Vapor Deposition (CVD) using MoO_3 and S as the precursors in a controlled way. Problems related with these methods are that to the difficulty in upscaling. Another bottom up approach, easier to upscale, is chemical synthesis [38].

Top down approaches vary from mechanical cleavage (time consuming and with low yield), liquid phase exfoliation, electron beam irradiation, plasmonic hot injection, and the most used method is lithium intercalation, generally using n-butyllithium has exfoliation agent, technique invented by Joensen in 1986 [39]–[41].

When using chemical synthesis, MoS_2 can be found in several forms, such as nanosheets, nanoflowers, and nanotubes all possessing different characteristics [32]. The different morphologies relate with strong anisotropy present in MoS_2, due to its unique layered structure. 2D materials show remarkable physical properties related to their thinner structure which bestows a change in electrical, chemical, mechanical and thermal properties such has larger surface area, quantum confinement effects that change band gap from indirect to direct, enhanced selectivity and sensitivity that makes it highly attractive for interlayer candidate in Li-S batteries [42].

Difference in electrical and optical properties evolve when reducing the number of layers by successful exfoliation. This results in band gap value increases, from bulk MoS_2 with a 1.1eV indirect bandgap, where valence band maximum (VBM) is at Γ point of Brillion zone and conduction band minimum (CBM) at middle between Γ and K points of Brillouin zone. The change to an 1.8 eV direct band gap where VBM and CBM coincide both at K point of Brillouin zone, is a consequence of quantum confinement and surface effects that emerge during this transition from bulk to monolayer [43].

2 Materials and Methods

2.1 MoS_2 exfoliation

2.1.1 Lithium Intercalation

The method used in this work, was solvothermal lithium intercalation, firstly demonstrated by Joensen in 1986 [40], [44], [45], it consists in the immersion of bulk MoS_2 in an organic lithium solution composed of ethylene glycol, used as the organic solvent and reductant media, mixed with lithium hydroxide that dissolves in the medium to create reduced Li^+ cations[46]. The solution is then placed inside a closed and pressurized reaction vessel (autoclave) and then taken to microwave where is heated under pressure, generating a high temperature and high pressure medium so Lithium ions, present in organolithium solution, insert between MoS_2 layers[47]. Layered structure of MoS_2, connected by weak Van der Waals bonds, establishes relative large interlayer spacing allowing alkali metal ions to be easily inserted between them, forming Li_xMoS_2 (Figure 2.1) [37], [40], [44], [46]. This is followed by a forced hydration exfoliation assisted by sonication.

The initial solution was prepared by adding 0.32g of LiOH into a 100 ml glass Becker containing 30ml of ethylene glycol. A small magnet was added into the organic solvent which was stirred for 5h to help dissolution. Followed by addition of 0.1g MoS2 powder (Sigma Aldrich) and stirred again for a 1h before being poured into a 50 ml Teflon protected autoclave. In order to intercalate lithium ions into MoS_2 layers slovothermal synthesis was performed for 3h, 5h and 10h at 180 ºC under 280 PSI at 200 watts power in a microwave oven (Microwave synthesizer – CEM Discover SP) [40], [46].

2.1.2 Forced hydration

Reaction between intercalated lithium Li_xMoS_2 and water generates lithium hydroxide (LiOH) and hydrogen gas (H_2) between layers of MoS_2. The release of H_2 helps layer separation eq 2.1, sonication is often used to assist (Figure 2.1) [40].

A strong polarity media abundant in cohesive forces like water performs great in MoS_2 exfoliation and behaves as good dispersion media for the sonicated MoS_2 flakes, which are charged and generate electrostatic repulsion in a polar solvent like water. [39], [48], [49].

Solutions resulting from lithium intercalation where previously washed, two times with acetone, via centrifugation at 12000rpm for one hour each to remove excess ethylene glycol from solution. Remaining acetone was dried in the oven at 50ºC during the night leaving only lithium intercalated MoS_2 (Li_xMoS2). Forced hydration was achieved when 25ml of water where added

to each synthesis and a sonication was performed for 0h, 2h, 5h and 10h, at 200 W, pulsed 10 seconds on 20 seconds off, immersed in an ice bath to control the synthesis temperature [40], [46].

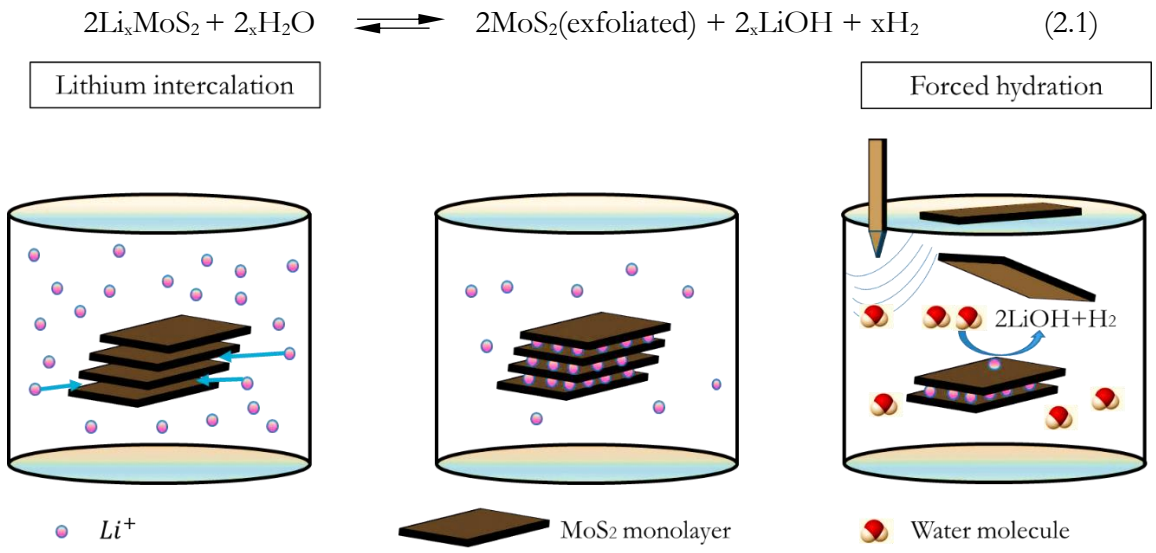

Figure 2-1 Representation of lithium intercalation process followed by forced hydration of MoS_2 samples

2.1.3 Exfoliated sample preparation

The samples resulting for the previous step were washed with water at 12000 rpm in a centrifuge for one hour after sonication. Un-exfoliated bulk particles where separated from exfoliated layers through a 4000 rpm centrifugation for 10 minutes, because exfoliated particles are smaller and tend to form a supernatant which was removed for characterization [46].

2.1.4 MoS_2 characterization

To understand the effects of lithium intercalation into MoS_2 different microwave synthesis where performed for 0h, 3h, 5h and 10h, giving rise to different composites of Li_xMoS_2. To perceive how sonication affected the intercalated samples each of the microwaved synthesis was sonicated for different times for 0h, 2h, 5h, 10h represented in table 1. By doing so, it was possible to understand how each step of lithium insertion and sonication is going to change the initial bulk MoS_2 layered structure and conductivity.

Characterization techniques that describe the material structure and electrical properties, before and after exfoliation, are ideal to learn about the alterations that happen in light of the approaches taken to convert the material to a 2D layer morphology. The characterization activities were performed in CEMOP and CENIMAT labs in FCT - Universidade Nova de

Lisboa, Portugal. Exfoliated MoS_2 was drop casted on a crystalline silicon substrate for SEM, DRX, and Raman analysis while it was taken in water suspension for spectroscopy analysis.

Measurements of lateral size where studied using dynamic light scattering (DLS), performed with AvidNano W130i equipped with 660nm laser diode. General shape and degradation of basal and edge planes as well has a perception of thickness was examined with scanning electron microscopy (SEM) (Zeiss Auriga CrossBeam Workstation). To grasp crystalline structure of MoS_2 was used XRD with X-ray diffractometer (PANalytical Xpert PRO MRD) using Cu K-alpha as X-rays source (wavelength 1.540598 Å). Raman microscope Reninshaw Qontor with a 532 laser beam, allowed for an understanding on the effects of lattice strain and Van der walls force interactions on crystal structure interface [50]. Studies of band gap, where analyzed with spectrometer UV-vis_NIR-Perkin Elmer lambda 950.

Table 1 description of the exfoliation methods performed in each sample

Sample	Exfoliation method
H0	Bulk MoS_2
H2	2h water sonication of bulk
H5	5h water sonication
H10	10h water sonication
3.0	3h solvothermal synthesis
3.2	3h solvothermal synthesis taken to 2h water sonication
3.5	3h solvothermal synthesis taken to 5h water sonication
3.10	3h solvothermal synthesis taken to 10h water sonication
5.0	5h solvothermal synthesis
5.2	5h solvothermal synthesis taken to 2h water sonication
5.5	5h solvothermal synthesis taken to 5h water sonication
5.10	5h solvothermal synthesis taken to 10h water sonication
10.0	10h solvothermal synthesis
10.2	10h solvothermal synthesis taken to 2h water sonication
10.5	10h solvothermal synthesis taken to 5h water sonication
10.10	10h solvothermal synthesis taken to 10h water sonication

2.2 Battery design

In order to have a good understanding on the effects of MoS_2 on limiting PS shuttling in Li-S batteries this work was focused on MoS_2 interlayers deposited on the cathode itself forming a double layer (DL) cathode. Another approach that was also studied, was the preparation of a MoS_2 layer covering the separator. Both methods were used in hope to capture PS that usually travel between the cathode and the anode to improve battery performance [22]. Thus, it was possible to study electrochemical changes in each cycle, for the first 100^{th} cycles.

Both, bulk and 3h synthesis sonicated for 10h exfoliated MoS_2 were used to create the two different interlayers placed in two different locations of the battery, (cathode double layer and coated separator).

Nonetheless another method was used to further understand physical blocking of PS. For that it was manufactured a DL made of 90% carbon black and 10% nafion acting as binder and DI water as the solvent, to cover the cathode in hope to prevent PS shuttle and diminish the solvent interaction with of first and second layer, to further explore the effects of different active material on PS trapping.

The behavior of Li-S cell's with each of these layers was compared with pristine cell, to understand the effects of the material, and the position of the layer, in the electrochemical performance of the cell, in the hope of making the Li-S battery more efficient.

The process consists of building a coin cell with a sulfur cathode, a Celgard separator a LiTFSI electrolyte a lithium anode and a MoS_2 interlayer (Figure 1.3).

2.2.1 Sulfur cathode

To obtain the standard sulfur cathode a 8-1-1 ratio was applied 0.12g of sulfur, the active material, and 0.06g of Carbon Black, the matrix that imprisons sulfur atoms, were both crushed on a mortar in the respective sequence, mixed together, and poured inside a 1.5ml Eppendorf. Then 0.12g of 10% PVDF in NMP, was added to the Eppendorf so CB could involve Sulfur inside its structure to create a porous structure to allow a good ionic conduction and trap PS. Then 1.2ml of NMP solvent was slowly added to reach the right viscosity, high enough not to create holes in the cathode during solvent evaporation, but low enough to be able to work with and spread evenly on to the aluminum current collector. The mixture was blended through ball milling at 30 Hz for 15 min to create a slurry with an (8-1-1) ratio. The resulting slurry was spread by film applicator on to aluminum sheet provided by Lithops, with a 200μm thickness

ensured by film applicator. The aluminum covered current collector was dried in the oven for 1h at 50ºC in order to evaporate the existing solvent [22].

2.2.2 Interlayer

Similarly, to what was done for the cathode, the 8-1-1 ratio was also used. In a mortar 0.06g of as-prepared MoS_2, representing 80% of active material, was mixed with 0.007g of CB and crushed in respective sequence, and then poured inside a 1.5ml Eppendorf, 0.07g of 10% PVDF in NMP solution and 200 µl of NMP added to achieve the right viscosity. Eppendorf was taken to ball milling at 30 Hz for 15 minutes, then film applicator spread the slurry with a 200µm thickness on the surface of sulfur cathode, forming an even height distribution. The coated cathode was taken to the oven, to dry the NMP, for 1h at 50ºC and cut into round shapes to dry in Vacuum at 40ºC for 4h inside a Büchi Glass oven B-585.

The same procedure was used to make the coated separator but instead of 200µm thickness was 70µm and the slurry was deposited on to the Celgard itself and then later dried during the night inside the hood. Then cut into round shapes and placed in a Büchi at 40ºC for 4h in vacuum.

To make the CB45 double layer 0.067g of was crushed in a mortar, mixed with 0.1712ml of nafion solution, dropped 100µl at the time, to achieve 90/10% ratio. The slurry was taken to film applicator and spread with to get 200 µm thickness on top of sulfur cathode. It was then cut into circular shapes and dried at 40 ºC in vacuum for 4h in the Büchi. The use of a different solvent was to prevent the dissolution of the first layer, consequentially mixing the cathode with the DL

2.2.3 Coin cell assembly

The batteries were assembled in a glovebox using a spring for compressing the layers together, improving contact between them. Lithium metal anode was placed at the bottom, followed by a Celgard 2500 layer has separator, covered with MoS_2 has interlayer, facing the cathode. On top of the Celgard was dropped 50µl of LiTFSI electrolyte and then the sulfur cathode previously prepared. The resulting coin cell was then compressed and closed.

2.2.4 Electrochemical characterization

To understand what was occurring with interlayer during cycling, five different types of interlayer contained cells where used and compared with one without any interlayer that was named "standard sulfur".

Three of these cells contained a second layer on top of the sulfur cathode one containing the bulk MoS_2 DL, another the exfoliated MoS_2 DL and the third CB45 DL.

Two other cells where designed with interlayer deposited on to the Celgard separator, one covered with bulk MoS_2 and the other with exfoliated MoS_2.

These batteries where taken to galvanometric capacity testing.

For ionic conductivity testing, three cells where made the standard one, and two with MoS_2 coated on the Celgard, one made with bulk and one with exfoliated.

Other three half cells were made, standard, bulk MoS2 DL and nafion solvent in carbon black DL. They were taken to cyclic voltammetry, except the one with exfoliated MoS_2 since the synthesis yield was too low to produce more during the time spent at Politecnico di Torino.

Nyquist plots and cyclic voltammograms performed for 5 cycles with a 10^{-4}(V/s) scan rate where both performed using CH Instruments 660D model while for galvanometric capacity and coulombic efficiency were performed 5 cycles at C/5 and the remaining 100 cycles at C/10 and coulombic efficiency where achieved by Arbin 96-channel battery tester.

All electrochemical analysis measurements where performed in Politecnico di Torino, Italy.

3 Results and Discussion

3.1 MoS_2 characterization

3.1.1 Flake size

With DLS it is possible to measure the hydrodynamic diameter present in a liquid suspension through light scattering, due to electromagnetic interference with the particles, in our case in a water suspension. Measurements are made for the hydrodynamic diameter of the particle meaning it measures the largest dimension. In the case of MoS_2 layered structure this corresponds to length which and will be addressed has flake size.

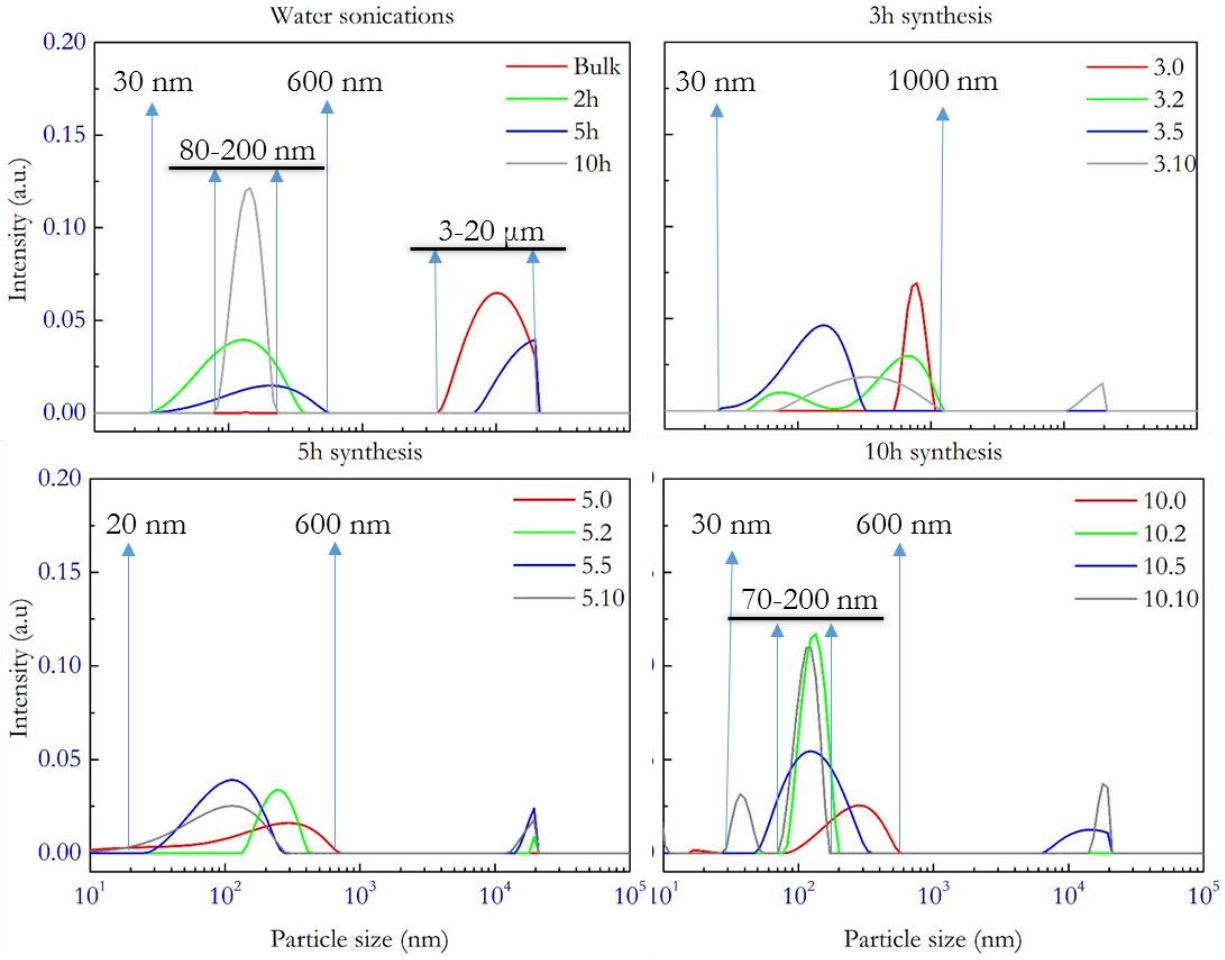

Figure 3-1 Dynamic light scattering graphics, comparing sonication times for 0h synthesis, 3h synthesis, 5h synthesis and 10h synthesis respectively a, b, c and d, each graph contains the information 0h, 2h, 5h and 10h sonication's represented respectively by red, green, blue and grey

Table 2 Average flake size and standard deviation for each sample's DLS measurements

Sample	Average flake size (nm)	Standard deviation
Bulk	**9788**	**4763**
H2	128	94
H5	59	46
H10	**140**	**43**
3.0	**766**	**150**
3.2	349	317
3.5	54	75
3.10	**398**	**316**
5.0	**549**	**436**
5.2	76	103
5.5	66	68
5.10	**73**	**74**
10.0	**167**	**142**
10.2	127	33
10.5	149	82
10.10	**51**	**42**

Sigma Aldrich reports a particle size provided in between 6μm to 40μm for the bulk MoS_2 untreated material while, in DLS reveals a lateral size ranging between 4μm to 21μm. With this particular DLS equipment, for suspension particles above 1μm in hydrodynamic diameter sensibility of the equipment is loss, therefore results are not so reliable.

In figure 3.1 are presented the DLS measurements for all synthesis performed. For 0h synthesis graph (figure 3.1a), it is possible to observe the effects of sonicating time. In 2h it is already possible to observe a reduction in lateral size compared with untreated material revealed by the change of average flake size (see in table 2) . The flakes dimension ranges from 30nm to 300nm, meaning particles where indeed reduced in lateral size as a result of sonication. After 10h sonication it is possible to see a more intense peak with an average flake size of 144 nm, revealing that exfoliation successfully reduced the size of present MoS_2 and concentration of material is higher than for other samples.

Comparing for different solvothermal synthesis times, for 0h of sonication represented in red, it is possible to see the effects of lithium intercalation and the relation of this procedure with lateral size of MoS_2 suspended flakes. A reduction of the average flake size values from 766nm

present in 3h synthesis, to 167 nm for 10h synthesis reveals tendency to reduce the lateral size of flakes with increasing synthesis time, revealing energy provided by microwave is breaking the flakes into smaller dimensions, which can also relate to a successful intercalation of lithium.

After insertion, exfoliation happens when intercalated lithium reacts with water, sonication helps to increase this interaction further separating the layers, so comparing diverse sonication times helps us perceive how the layers are separated from each other after intercalation.

Generally, sonication helps to produce smaller particles for intercalated MoS_2, noticeable from samples that were submitted to any sonication (2h,5h,10h) compared to those that were not sonicated (0h). It was observed particle size range always decreases with this effect. This is a result of increased sonication energy provided to the solution which fractures the flakes into smaller ones, leaving suspension hydrodynamic sizes smaller.

3.1.2 Morphology

Scanning electron microscope surface analysis provides detailed images of MoS_2 morphology, scaling up to 300 thousand times the real image and with resolutions up to 3.5nm providing a perception of layer size, stacking and edge formation.

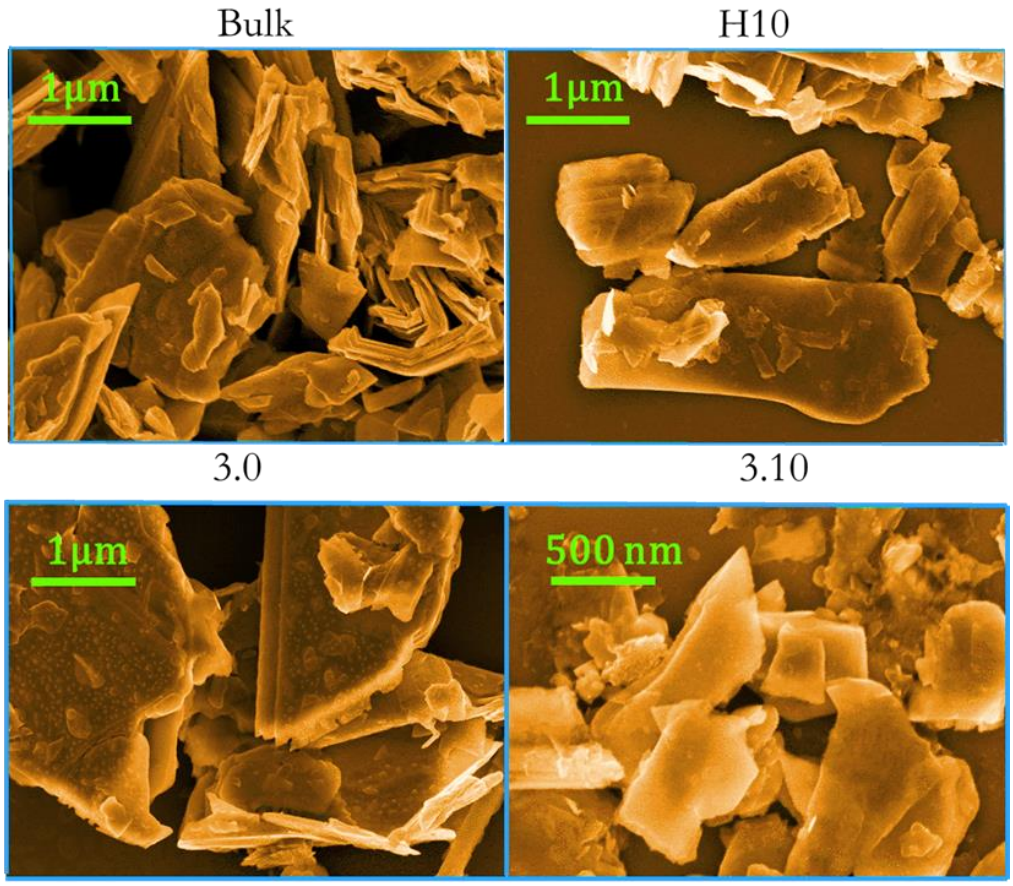

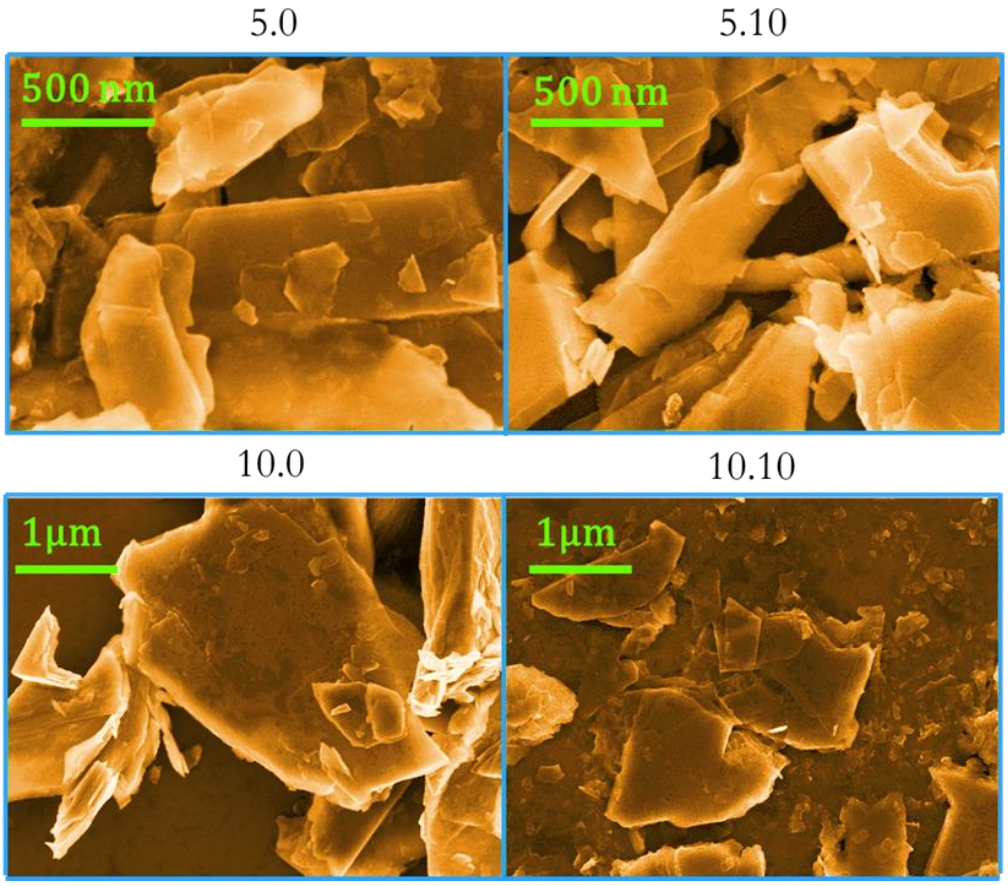

Figure 3-2 SEM images from bulk, 10h water exfoliation, 3h synthesis sonicated for 0h and 10h, 5h synthesis sonicated for 0h and 10h and 10h synthesis sonicated for 0h and 10h.

In Figure 3.2 are presented SEM images of the samples made previously. The image for bulk sample exposes the initial state of the powder received from sigma Aldrich before any treatment. It is possible to observe a huge stacking of MoS_2 layers compressed and curled with average measured length of 1.47 µm and standard deviation of 785 nm (consistent DLS analysis), and some larger flakes that couldn't fit in the image.

In 10h water sonicated sample (H10), exfoliated MoS_2 flakes are flat side up, not in a compressed way. Suggesting that some layers broke and separated trough sonication creating more space between flakes. Moreover, average size of the flakes was 938 nm and a standard deviation of 1 µm.

Observing the images and non-sonicated samples (3.0, 5.0 and 10.0) it is possible to observe an average flake size similar to bulk sample for 3.0 sample and a reduction of average size with the increase of synthesis time 296 nm and a standard deviation of 252 nm for 5.0 sample, less concentration and less curling at the edges possibly as a result of insertion of lithium into the structure that separated this curled edges, 10.0 sample as higher average size but also higher standard deviation 1.27 µm and 1.29 µm respectively. It is still observable some stacking of layers that means that intercalation had some effect MoS_2 but wasn't enough to produce monolayers.

For samples that suffered from lithium intercalation and then sonication, 3h synthesis sonicated for 10h resulted in flakes with a fewer number of layers which is attributed to a thinner structure that allows for electrons in SEM to interact with the flakes below. For the 10h synthesis and 10h sonication a lot of very small sheets are observed (consistent with DLS analysis), average of 406 nm and a standard deviation of 394 nm, probably a outcome of the big amount of energy that was transferred into the flakes, both microwave from intercalation and energy from sonication, breaking original bulk into very small flakes [36], [46].

Using SEM it is not possible to determine the number of layers but the surface area of the intercalated samples increased.

3.1.3 Crystallographic structure

X-ray diffraction can reveal details in the internal structure of crystals in the order of 10^{-10} m, near the wavelength of the actual X-Ray used for these measurements. It is used to determine atomic structure of a crystal and the interlayer spacing, a result of interference of atomic crystal structure with the incident X-rays, that get diffracted into different directions [51].

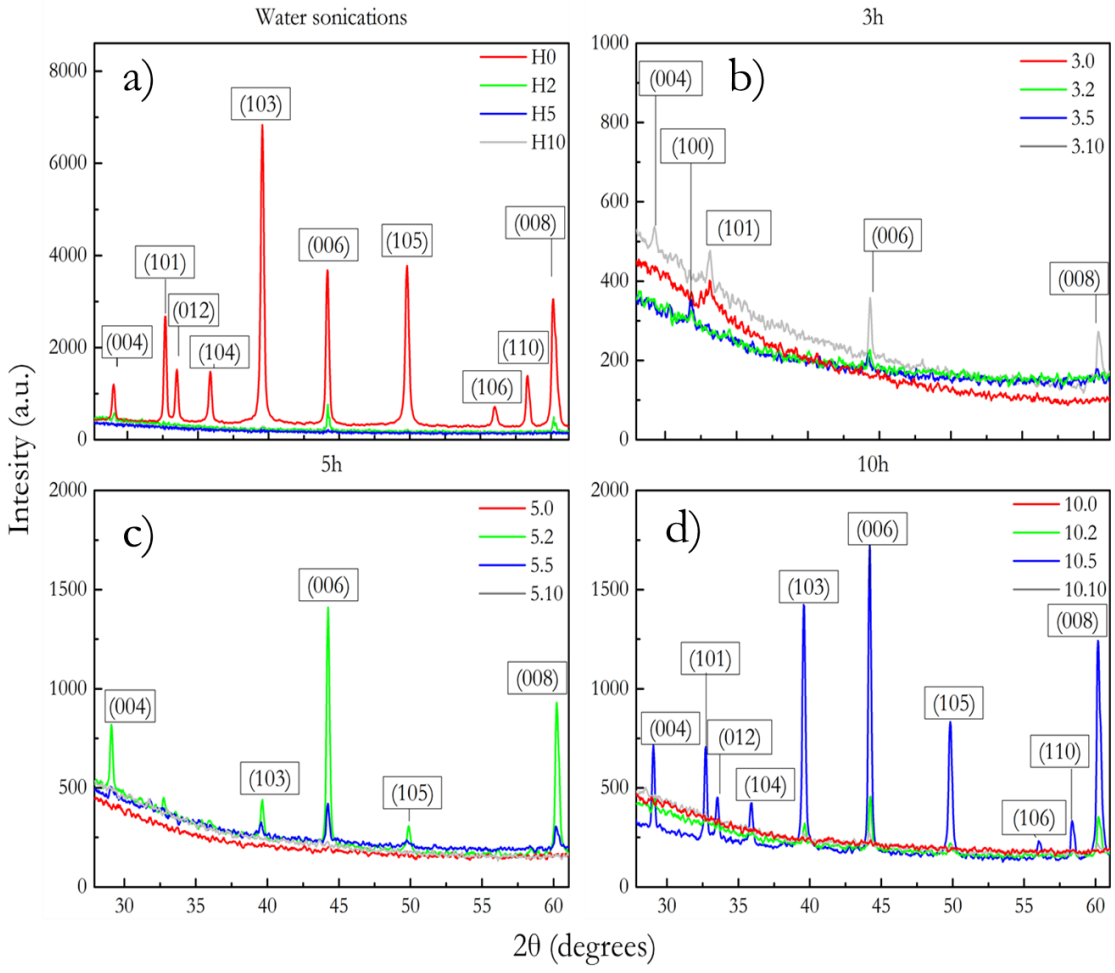

Figure 3-3 XRD diffractograms for different synthesis times, 0h, 3h, 5h, and 10h respectively a, b, c and d

Figure 3.3 shows the diffractograms for all samples of MoS_2, with a representation also of the peaks for bulk that relate to a 2H structure, while in figure 3.5 only the most intense peak related with (002) plans are presented (the only peak visible for all samples) [52], [53].

For non-synthetized water sonicated samples (see figure 3.3a) most of the 2H peaks vanish with sonication. For 2h sonication (006), (004) peaks related with 2H structure are still detected. However, for further sonication these peaks disappear, and this is attributed to cracking of MoS_2 initial structure diminishing the number of diffracted X-rays in each direction.

For 3h synthesis (figure 3.3b) besides (002) peak, only (101) peak is also present. This is a good indication that samples suffered from intercalation because 2H structure related peaks are gone when the synthesis time increase since any other peak disappears beside (002).

When samples were sonicated after synthesis some of the peaks corresponding to 2H structure become more intense. This is a result of a reaction of water with lithium liberating intercalated lithium from the structure and allowing MoS_2 structure to return to its 2H form [52], [54].

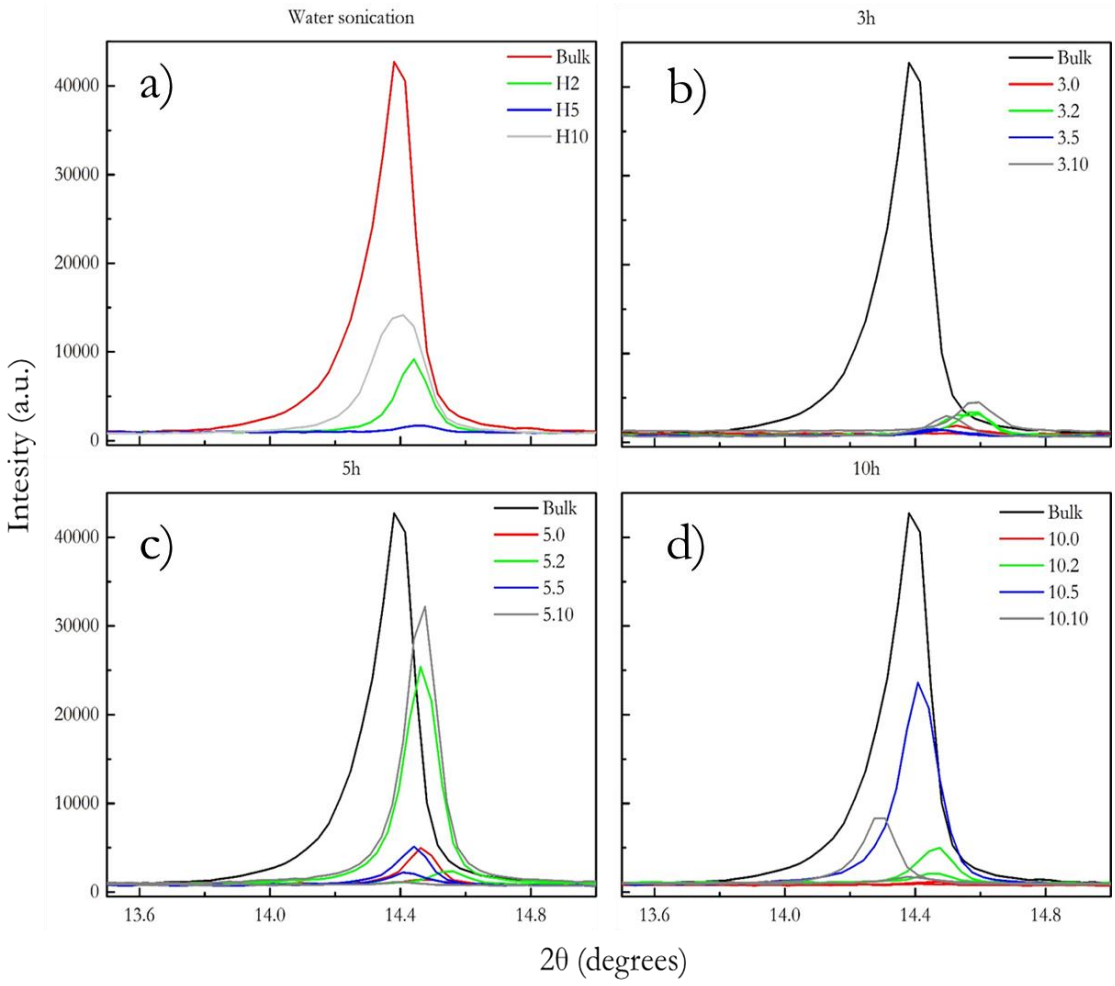

Figure 3-4 XRD diffractograms of (002) peaks for different synthesis times, 0h, 3h, 5h, and 10h respectively a, b, c and d

Through Bragg's law (eq 3.1) it's possible to determine the distance between lattice plans (d) which depends on the angle of the diffracted X-ray (θ), and on the wavelength of the electromagnetic radiation in this case X-rays with (λ) 1.5406 Å. Analyzing the most intense peak of MoS_2 (002) it is possible to know what is occurring between the atomic plans inside the crystalline structure of MoS_2 [51], [55].

$$2d\sin(\theta)=\lambda \tag{3.1}$$

As it was referred before, MoS_2 as a 2H (hexagonal) structure, which means structure can be dimensioned by two lattice parameters (a) and (c) described in figure 3.5.

Dimensions of MoS_2 crystal are calculated through inter-planar spacing equation (eq 3.2). Orientation (002) was chosen because it has the highest peak intensity. The (h,k,l) are miller index associated with peak orientation, (h=0; k=0 and l=2). To calculate c, we need d-spacing values, previously calculated and eq 3.3 can be used in the case of (002) orientation.

$$\frac{1}{d^2}=\frac{4}{3}\left(\frac{h^2+hk+k^2}{a^2}\right)+\frac{l^2}{c^2} \tag{3.2}$$

$$<=>$$

$$\frac{1}{d^2}=\frac{l^2}{c^2}$$

$$<=>$$

$$c=\sqrt{d^2l^2} \tag{3.3}$$

After calculating lattice parameter c. It is possible to solve the equation 3.2 and calculate lattice parameter (a). Relying on the second most intense peak of MoS_2 (103), and therefore replacing the miller indexes (h=1; k=0 and l=3).

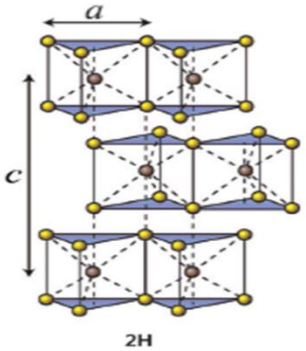

Figure 3-5 Representation of MoS_2 atomic structure and lattice parameters a and c of an hexagonally close-packed MoS_2 structure figure extracted from [56].

Table 3 Values of interlayer spacing and lattice parameters c and a for some of the exfoliated samples.

	$d_{(002)}$ (Å)	c (Å)	a (Å)
Bulk	**6,147**	**12,29**	**3,161**
H2	6,130	12,26	3,107
H5	6,124	12,25	-
H10	**6,149**	12,29	3,155
3.0	**6,176**	**12,35**	**3,162**
3.2	6,176	12,35	3,158
3.5	6,147	12,29	3,169
3.10	**6,147**	**12,29**	**3,158**
5.0	**6,197**	**12,39**	**3,163**
5.2	6,142	12,28	3,164
5.5	6,142	12,28	3,164
5.10	**6,154**	**12,31**	**3,164**
10.0	6,127	12,25	-
10.2	6,122	12,24	3,166
10.5	6,142	12,28	3,159
10.10	6,194	12,39	3,162

Figure 3.4 shows the (002) peaks for each exfoliation. When water sonication is performed on bulk MoS_2, the peaks tend to decrease in intensity, which is typically ascribed to decrease in number of layers in MoS_2.

For non-sonicated samples (represented in red) that were intercalated with lithium just very low intensity peaks are observed. When these intercalated samples are sonicated the intensity increases, which can be a repercussion of the way exfoliated MoS_2 is extracted from water solution. Since the sample is centrifuged to separate bulkier particles from exfoliated, present on supernatant, the concentration of smaller particles present on the surface of the liquid increased, rendering more intense peaks [44], [51], [55].

Bulk interplanar spacing (d=6.147 Å) and lattice parameters (c=12.29Å and a=b=3.161Å) calculated and represented on table 1, was well accordingly to literature [52], [57]. The d-spacing values show that for the 3.0 and 5.0 synthesis distance between lattice planes was bigger than for bulk, which is consistent with the lithium intercalation occurring in the material. It was also

noticed that after exfoliation this value went back to regular interplanar spacing of MoS_2, which can indicate that lithium was still present inside the structure before sonication of the sample. In addition values for c lattice parameter increase accordingly with d-spacing, revealing a more elongated structure, consistent with effects of intercalation [57], [58]. For 10h synthetized sample sonicated for 10h (figure 3.5d) shows an increase of d-spacing and c lattice parameter, meaning intercalation of lithium effects remained even after sonication of the samples which also happens for 10h sonication of 5h synthesis [50], [52], [55], [57], [58].

3.1.4 Raman scattering

When monochromatic light is irradiated on to a surface sample produces scattered light, some of these scattered photons maintain the same frequency as the source of incident light, the so-called Rayleigh scatter. Raman scatter happens when photons interact with the sample phonons and change their frequency because of an energy exchange. There are two types of Raman scatter, when some photons lose energy transferred to a phonon that is in the ground vibrational state and changes to a higher vibrational frequency, known as a stokes transition, and another transition in which the photon gains energy from the phonon that transits from a higher vibration level to a lower vibrational frequency known as anti-stokes [59].

The two main MoS_2 peaks studied in literature are the $E_2{}^1g$ and A_1g because peak frequency is layer dependent.

$E_2{}^1g$ peak corresponds to an in-plane vibration of an S-Mo-S layer against adjacent layers where sulfur atoms of different layers move in opposite directions (figure 3.6).

A_1g mode is an outcome of out of plane vibration, a reaction of displacements of S atoms on opposite directions, motion perpendicular to the layer plane (figure 3.6) [60].

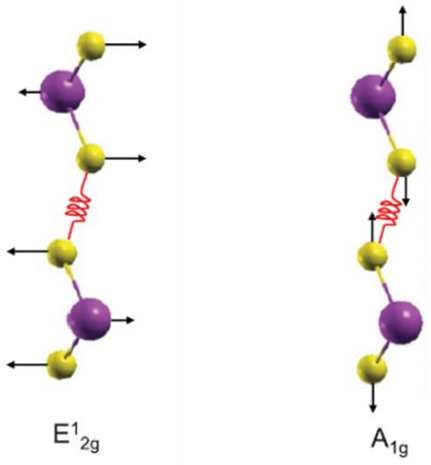

Figure 3-6 Representation of Raman vibration modes of MoS_2, image adapted from reference [60]

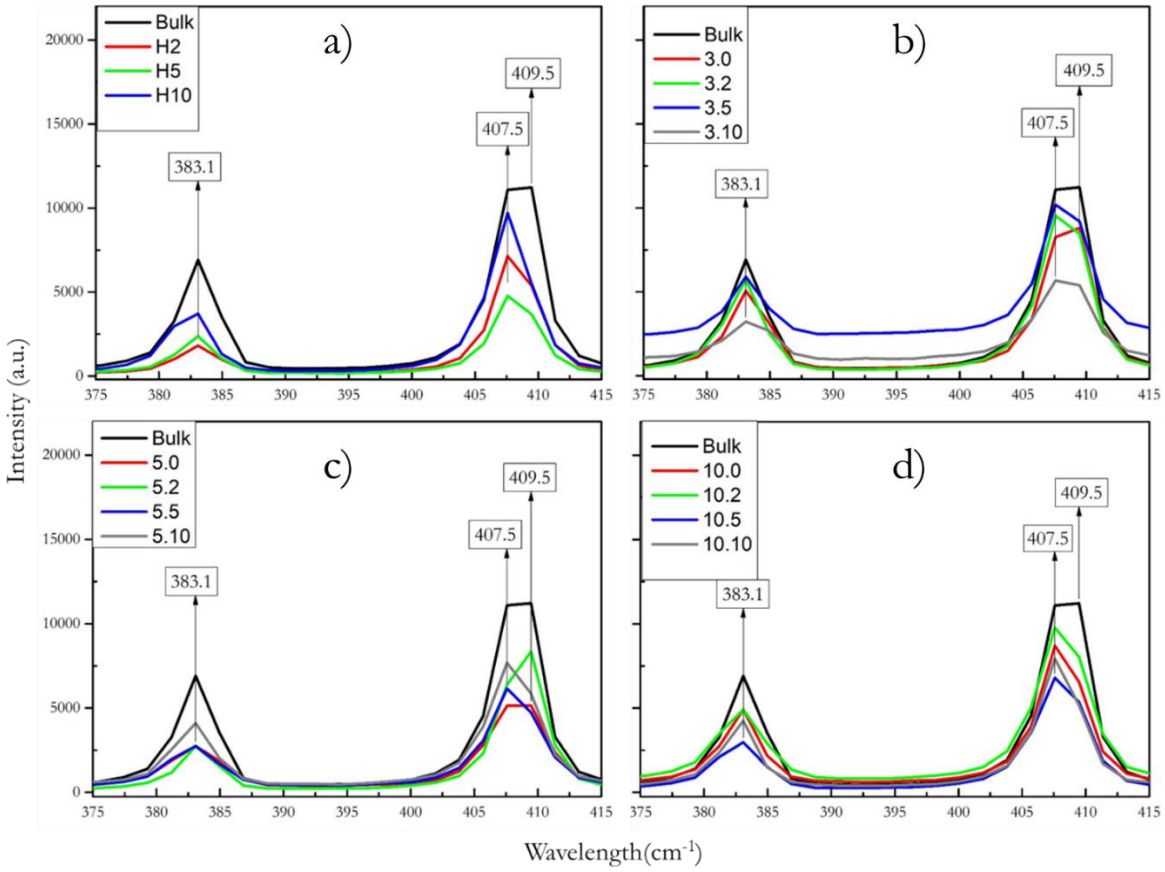

Figure 3-7 Raman graphics of each sample of MoS_2 0h, 3h, 5h and 10h synthesis respectivly a,b,c and d

From figure 3.7a corresponding to water sonication's, is possible to observe A_1g peak position 409.5 cm^{-1} present in bulk sample, that changes to 407.5 cm^{-1} in sonicated samples. The lower vibration frequency is a possible a repercussion of an increase of atom vibrations inside MoS_2 due to lower force constants affecting this vibration, mainly composed of Van der Walls forces that connect each layer. Therefore, a shift to lower frequencies might be related to a smaller number of layers present. This decrease of frequency is observed in almost all exfoliated samples, that can indicate a reduction in the number of layers, but it does not necessarily imply that monolayers are obtained from exfoliation.

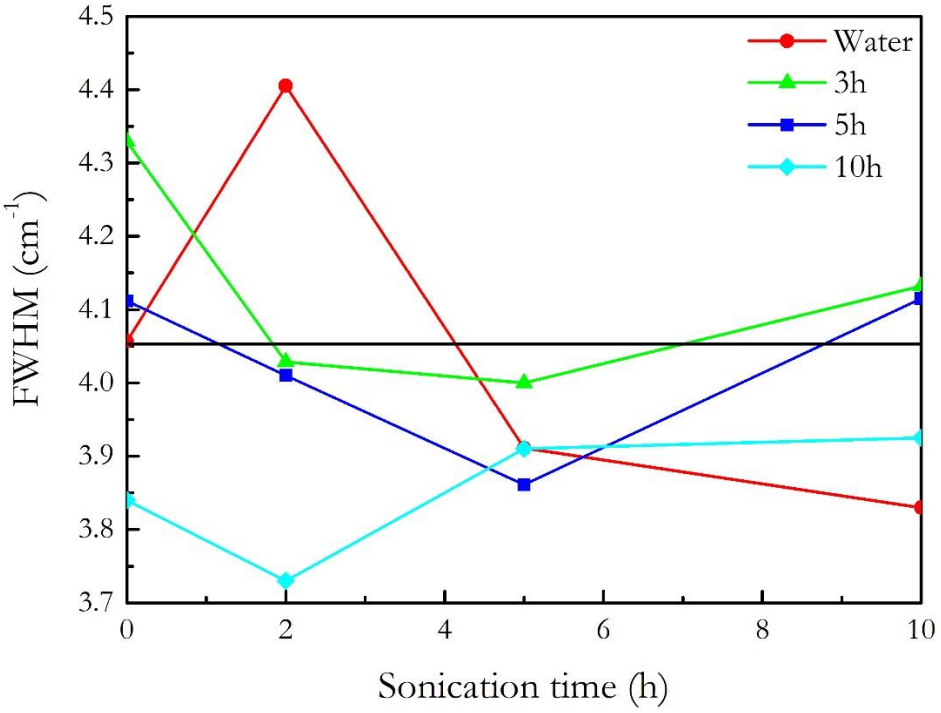

Figure 3-8 FWHM values of A_{1g} Raman peaks

Full width at half measure (FWHM) was determined for each A_1g peak because it is often associated with number of layers present in the material. The black line across the graphic represents the FWHM for bulk material. For non-sonicated samples 3.0 and 5.0 the band width is larger than for bulk, which is also observed for same synthesis and sonicated for 10h, that was related to a decrease in the number of layers [61], [62]. These Raman results are consistent with XRD ones, which show that 3.0, 5.0, 3.10 and 5.10 samples where the most affected in exfoliation being good indicators that where successfully exfoliated.

3.1.5 Band gap

Band gap properties of MoS_2 change when going from bulk to monolayer (see figure 3.9). MoS_2 is considered bulk when the number of layers is equal or superior to 7, below that number, material starts to behave differently because of quantum confinement effects.

Bulk MoS_2 has an indirect band gap of about 1eV gap. Conduction band minima (CBM) is present somewhere between Γ and K points of Brillouin zone, and valence band maxima (VBM) is located at Γ point of Brillouin zone, as is demonstrated in figure 3.10 [63].

Conduction band states at K point are mostly comprised of strongly localized d orbitals of Mo atoms which have reduced interlayer coupling, since Mo atoms are localized between S atoms in MoS_2 structure, that results in K point conduction band states hardly changing when reducing number of layers, as we can observe in figure 3.9.

On the other hand, states near Γ point of Brillouin zone are formed by a combination of d orbitals of Mo metallic atoms and anti-bonding p_z orbitals of S atoms. When number of layer reduces, also the interlayer interaction reduces, therefore Mo d_z^2 and p_z states that have strong interlayer coupling shift to lower energies, and CBM and VBM both coincide in K point of Brillouin zone [34], [64].

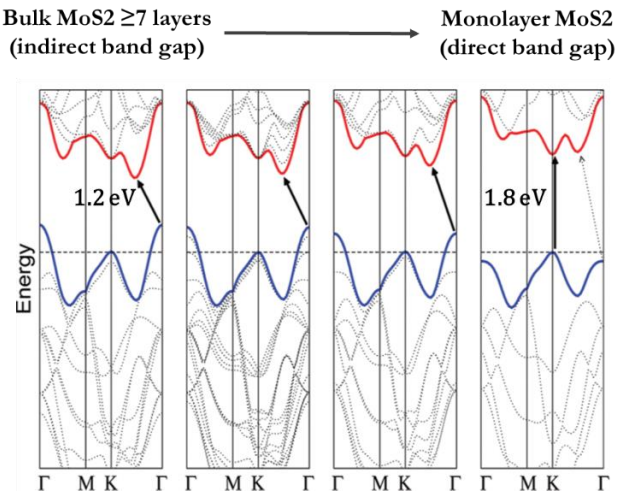

Figure 3-9 Representation of band gap transformation on MoS_2 picture adapted from reference [34]

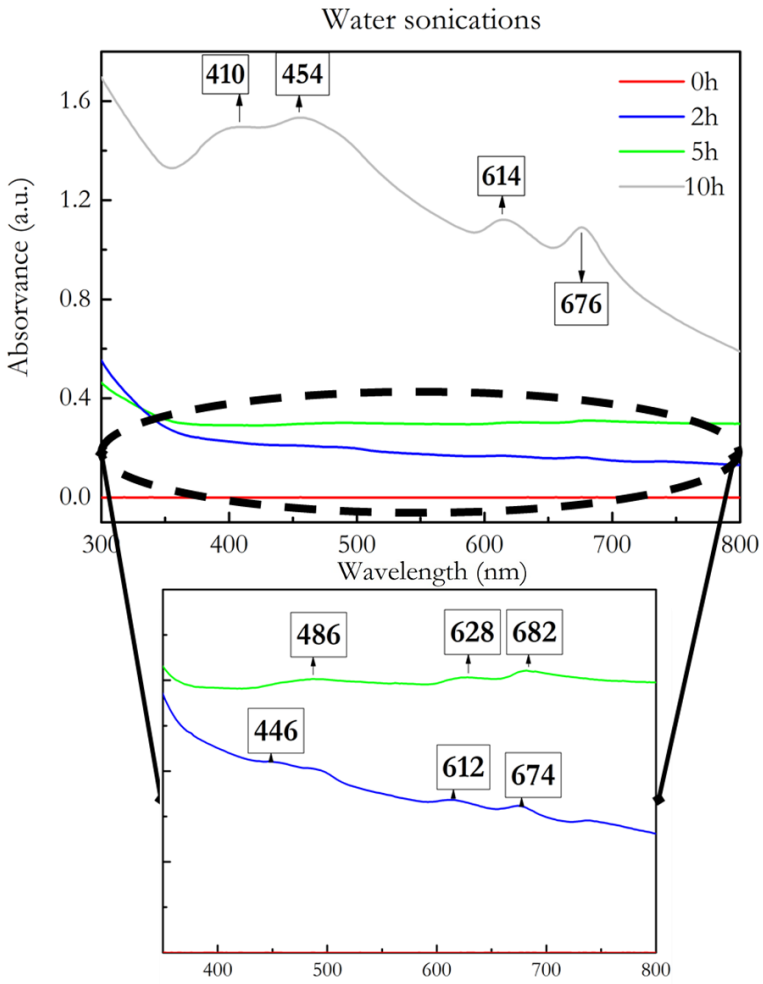

Figure 3-10 Optical spectroscopy graphics of water sonication of MoS_2

When the samples are sonicated, we start to observe some absorbance peaks for MoS_2, this means samples suffered from quantum confinement effects and band gap changed.

Usually A and B excitonic peaks, around 670nm and 610nm respectively are related to direct band transitions in K point of Brillouin zone. The increasing intensity of these peaks with more sonication time is probably related with the increase of concentration of sample measurements due to a larger number of particles that where successfully exfoliated figure 3.11.

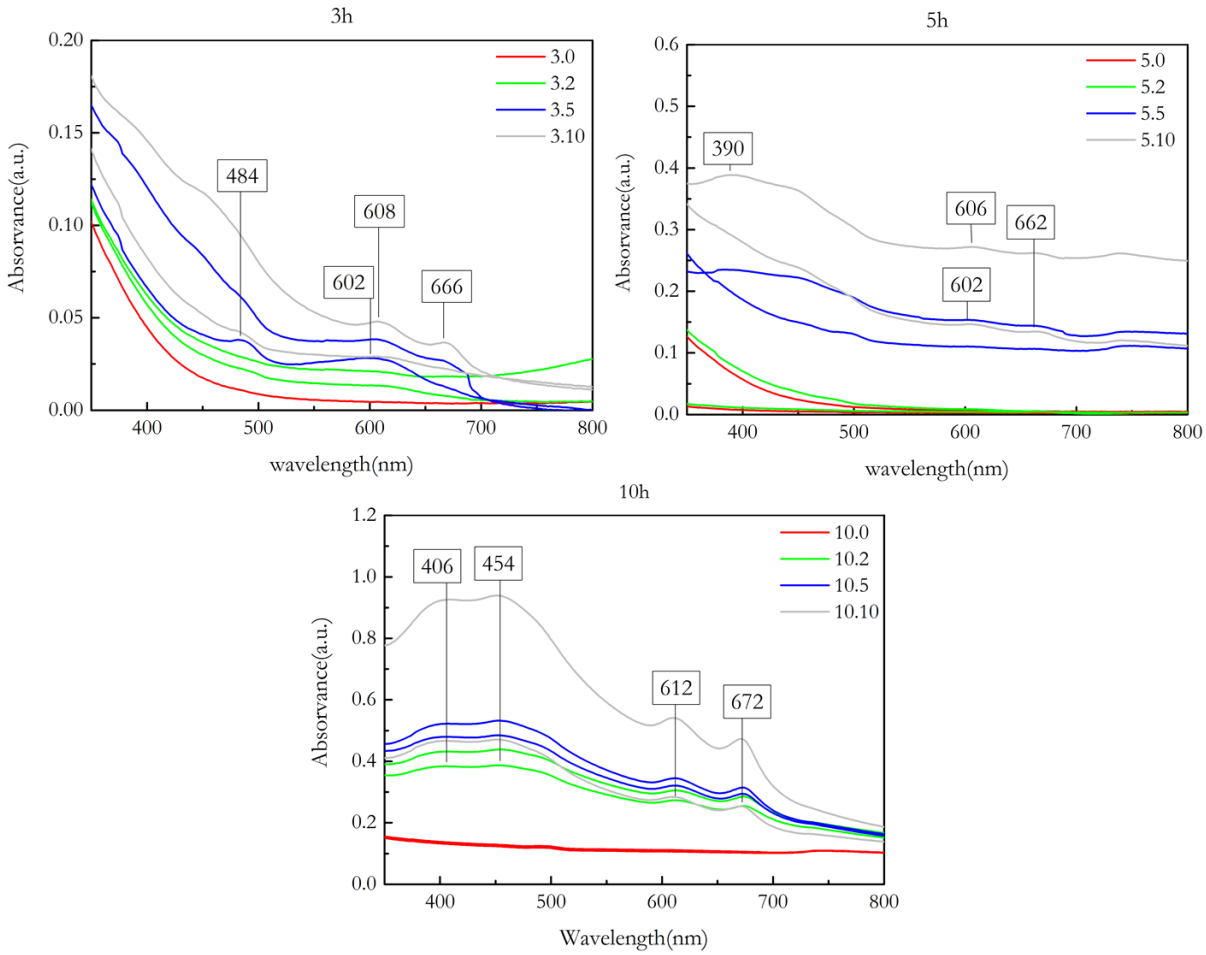

Figure 3-11 UV-vis optical spectroscopy graphs performed on 3h, 5h and 10h synthesis of MoS_2

In Figure 3.11 in red are compared all synthesis performed to MoS_2 before they were taken to sonication, in which no peak is observed, that means the material is an indirect band gap semiconductor, this is a result of what we already had concluded in previous XRD, Raman and SEM analysis, that lithium is still intercalated into the structure.

When sonicated the synthesis, we can start to observe some increase in peak intensity consistent with increasing the sample concentration which relates to more amount of material being successfully exfoliated [39].

When increasing the synthesis time, we can observe that peaks are more intense and with more definition, and for 10h synthesis the appearance of additional peaks around 406nm and 450nm, attributed to C and D excitonic peaks. This peaks correspond to higher energy transitions that result from band nesting effect, this is an effect of lithium intercalation that tends

to provide electrons to MoS_2 structure, increasing electron density in the d orbital of Mo atoms, destabilizing semiconductor structure to 1T phase, this reveals that synthesis time helps layers to separate and increases quantum confinement effect [65][45].

Blue shifts are linked to geometrical confinement of excitons a consequence of decreasing the number of layers. The 3h and 5h synthesis sonicated for 10h the largest blue shifts among all samples with values of A and B excitons of 666nm and 608nm for 3h synthesis and for 5h synthesis 662nm and 606nm respectively [48], [63]. This change in the peaks might be related with decreased layer number which consistent with previous analysis performed on the samples.

3.2 Electrochemical characterization

3.2.1 Ionic conductivity

Electrochemical Impedance analysis, results from applying an AC signal potential trough an electrochemical cell changing the original AC electromagnetic wave. Applying a sinusoidal potential excitation through the cell will generate a similar sinusoid at the same frequency but with difference in amplitude and phase from the original signal input.

From gain and phase of resulting wavelength is possible to extract polar coordinates and perform a Nyquist plot wherefrom is possible to perceive impedance behavior of the cell [66].

This case EIS analysis was performed on the separator coated with different materials (see figure 3.12).

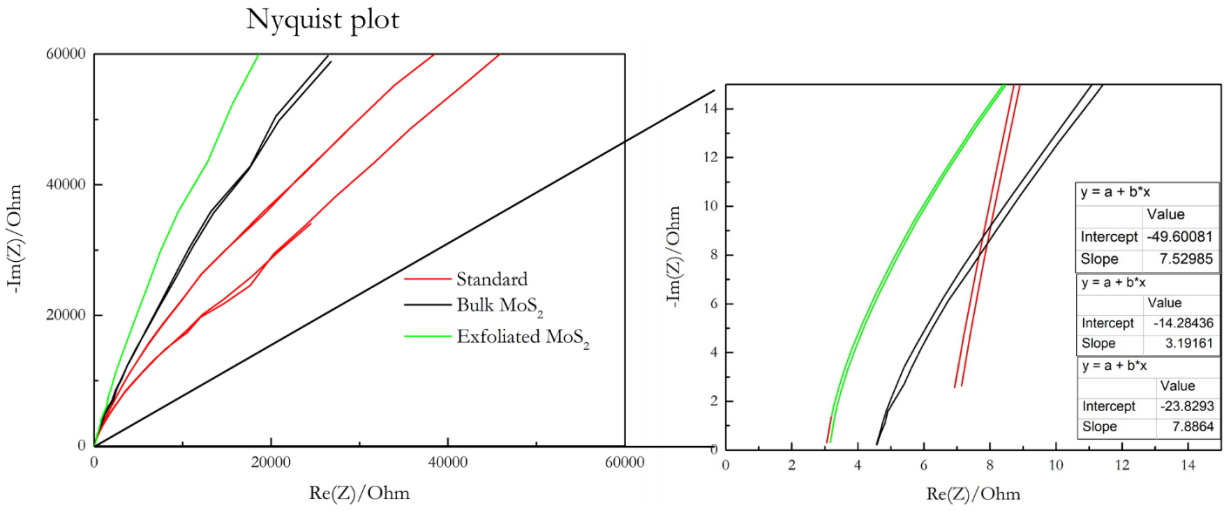

Figure 3-12 Nyquist plots performed on coated Celgard separators

Interception of the values of each line with the real axis of the Nyquist plots is attributed to solvent resistance of electrolyte (Rs). When fitting all curves for each type of separator is possible to determine that pristine Celgard separator presents a resistance of 6.6 Ω, that decreases for the

Bulk MoS_2 coated separator reaching a value of 4.5 Ω, and surface resistance got down to 3 Ω for the exfoliated MoS_2 (3h synthesis 10 sonication) coating (see figure 3.12). This improvement is a consequence of good contact between exfoliated MoS_2 and electrolyte, thus conduction of lithium ions through the separator is actually improved because the reduced viscosity of the electrolyte, a feature accomplished by the ability of blocking the soluble polysulfides of MoS_2 material. The increased surface area in exfoliated MoS_2 improves contact, thus increasing conduction of lithium ions [67]–[69] .

3.2.2 Cyclic voltammograms

Cyclic voltammetry is a common tool used to understand electron transfer processes of electrochemical cells, performed in Li-S batteries to study electrochemical reversibility, cycle stability, polarization and understanding the amount of sulfur being used for energy storage.

A working electrode performs a linear sweep of potential per unit of time, known as scan rate, until a set potential is reached, then is scanned in the opposite direction. Potential is measured between working electrode and reference electrode, current is measured between working electrode and a counter electrode and plotted with voltage as the independent variable, resulting in a cyclic voltammetry trace used to study electrochemical properties [70], [71].

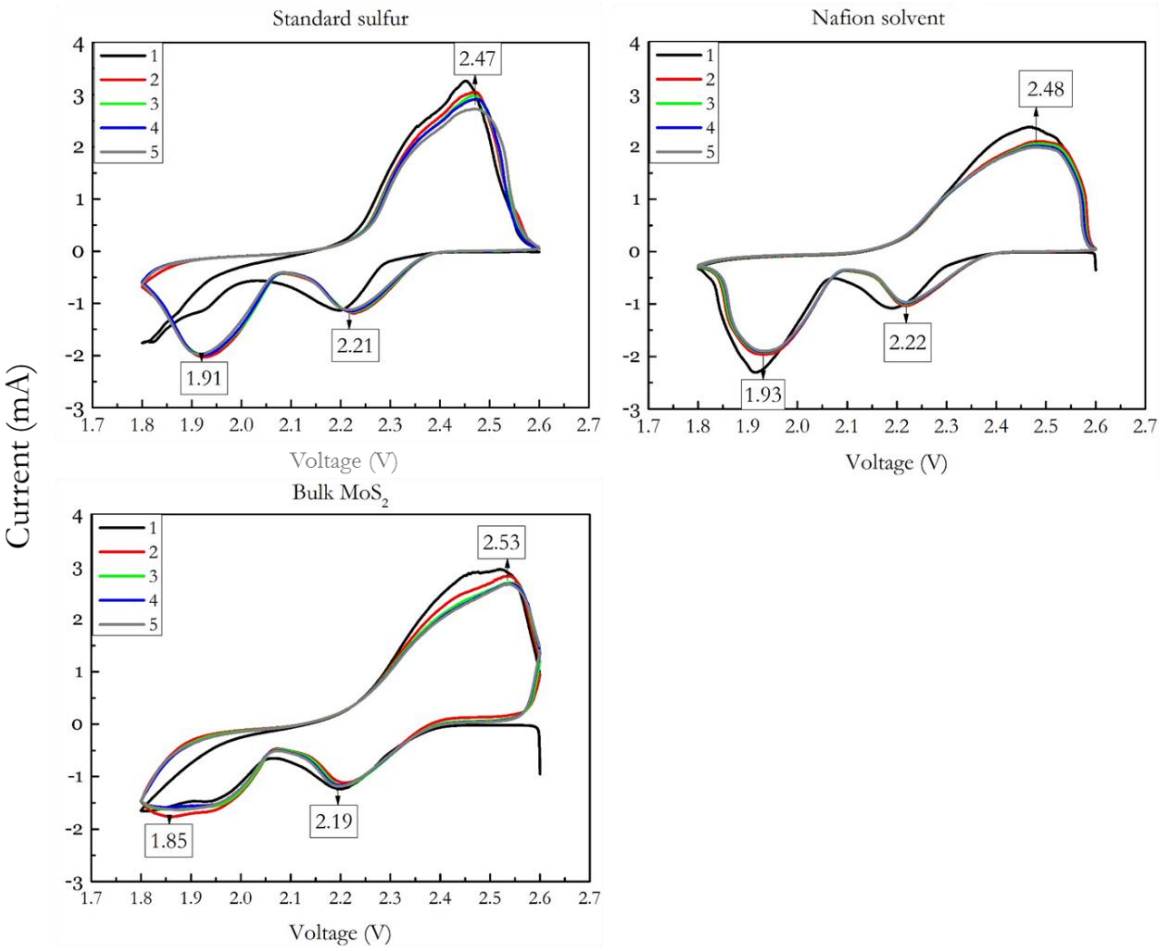

Figure 3-13 Cyclic voltammetry performed on sulfur batteries, one standard one with a Nafion solvent and carbon black double layer and one with a bulk MoS_2 double layer

Is possible to observe in the cathodic scan the two distinct peaks for standard sulfur battery (see figure 3.13), one present at 1.91 V which correlates to the reduction of elemental sulfur to high order lithium polysulfides, Li_2Sn ($4 \leq n \leq 8$), and a second peak present at 2.21V that matches the further reduction of PS into lower order PS such as Li_2S_2 and eventually Li_2S.

Anodic scan reveals a single peak present at 2.47V but much larger in width, that is a repercussion of both oxidation reactions happening so close together, this peaks are associated with oxidation of Li_2S to Li_2S_2, which oxide to high order PS and process continues until lithium polysulfide is completely converted in to elemental sulfur [10], [22], [67], [72].

Anodic peak separation between reaction peaks for standard sulfur is 0.3V, for double layer bulk MoS_2 peak separation is 0.34V and for nafion solvent based double layer, separation between peaks is of 0.29V. The lowest peak separation of CB nafion solvent DL, is a good indication of electrochemical reversibility of PS [9],[22].

On another side, cyclic voltammetry of bulk MoS_2 demonstrates high consistency between each cycle curve, and even higher consistency is shown in CB nafion DL, which relates to lower

polarization and a better cycle performance for this kind of batteries meaning that for each cycle battery loses less capability of sulfur utilization than the standard sulfur battery [5].

So even though standard sulfur batteries show better electrochemical reversibility good ionic and electron transport, the addition of the double layer promises a better cycle stability and longer battery life for Li-S batteries.

3.2.3 Galvanometric capacity

The number of hours required to perform a complete discharge of its theoretical discharge value is expressed as C-rate. Theoretical Capacity of a sulfur battery is 1672mAh/g, a discharge of this capacity over a period of 10h is known as C/10 meaning 0.1672A per hour, and over a period of 5h known as C/5 meaning 0.3344A per hour.

In our case 5 cycles were performed at C/10 and the remaining cycles at C/5.

When battery reaches end of discharge (EOD) output voltage reaches its minimum safe threshold and the battery as reached its maximum discharge capacity value for that cycle.

In figure 3.13 we can observe galvanometric capacity graphs performed at C/10, where for all graphs was possible to observe two discharge capacity plateaus, first one corresponding to conversion of sulfur to high order PS which contributes about 25% of total capacity and a lower order plateau dominated by the conversion of high order polysulfides into low order polysulfides, which contributes to 75% of the capacity [15].

Lower plateau is wider, due to slow kinetic reactions from soluble S_4^{2-} to insoluble Li_2S_2/ Li_2S, therefore curve takes longer to discharge, up to a point the cathode gets covered by non-conducting Li_2S_2/ Li_2S polysulfides, reducing the amount of charge transfer paths and leading to a fast decay in voltage resulting in the reaction's end of discharge.

EOD values are related to the amount of sulfur being reduced to produce electrons that generate current.

At the first cycle at C/10, standard sulfur battery is at 66% of theoretical discharge capacity, as for nafion solvent DL is at 75%, Bulk MoS_2 DL was at 64% and exfoliated MoS_2 DL 70% showing improvement over bulk. The highest efficiency was achieved adopting a different solvent for the DL, which is probably related to the fact that using the same solvent interacts with the first layer and mixes with the second layer. Still exfoliated MoS_2 sample showed some improvement over standard sulfur battery. The increase in EOD means the amount of sulfur being reduced is higher, thus barriers are working and blocking polysulfides from shuttling [15].

For depositions on Celgard, bulk MoS_2 showed an improvement on discharge capacity, by using 76% of sulfur's theoretical capacity and exfoliated MoS_2 delivered a remarkable 77.5%,

acknowledging MoS_2 ability to blocking PS, increasing amount of sulfur utilization, this relates to exfoliated MoS_2 unique properties.

Kinetic reaction efficiency can be evaluated by the voltage difference (ΔE) between charge and discharge plateaus at 50% EOD.

In standard single layer battery, (ΔE) was determined to be 182mV. For nafion solvent DL the value is 153mV corresponding to a 16% decrease compared with standard Li-S battery. This decrease is related to improved ion transport paths and adsorption surfaces that promote better kinetics in this kind of batteries. In DL containing bulk MoS_2 the ΔE value is 222mV meaning slower electrochemical reactions. For exfoliated MoS_2 it is reached an impressive 100mV meaning a 45% improvement related with better kinetic reactions, due to high ionic and electronic transport paths and adsorption surfaces created by high surface area of exfoliated MoS_2 [5], [22].

Bulk MoS_2 coated Celgard demonstrated highest ΔE value of 247mV and the exfoliated sample 195mV showing that coating the separator was slowing kinetic reactions, possibly due to the addition of another surface layer where insoluble PS can create a non-conducting coating which blocks charge transfer paths and increases resistivity [5], [22].

3.2.3.1 C/10

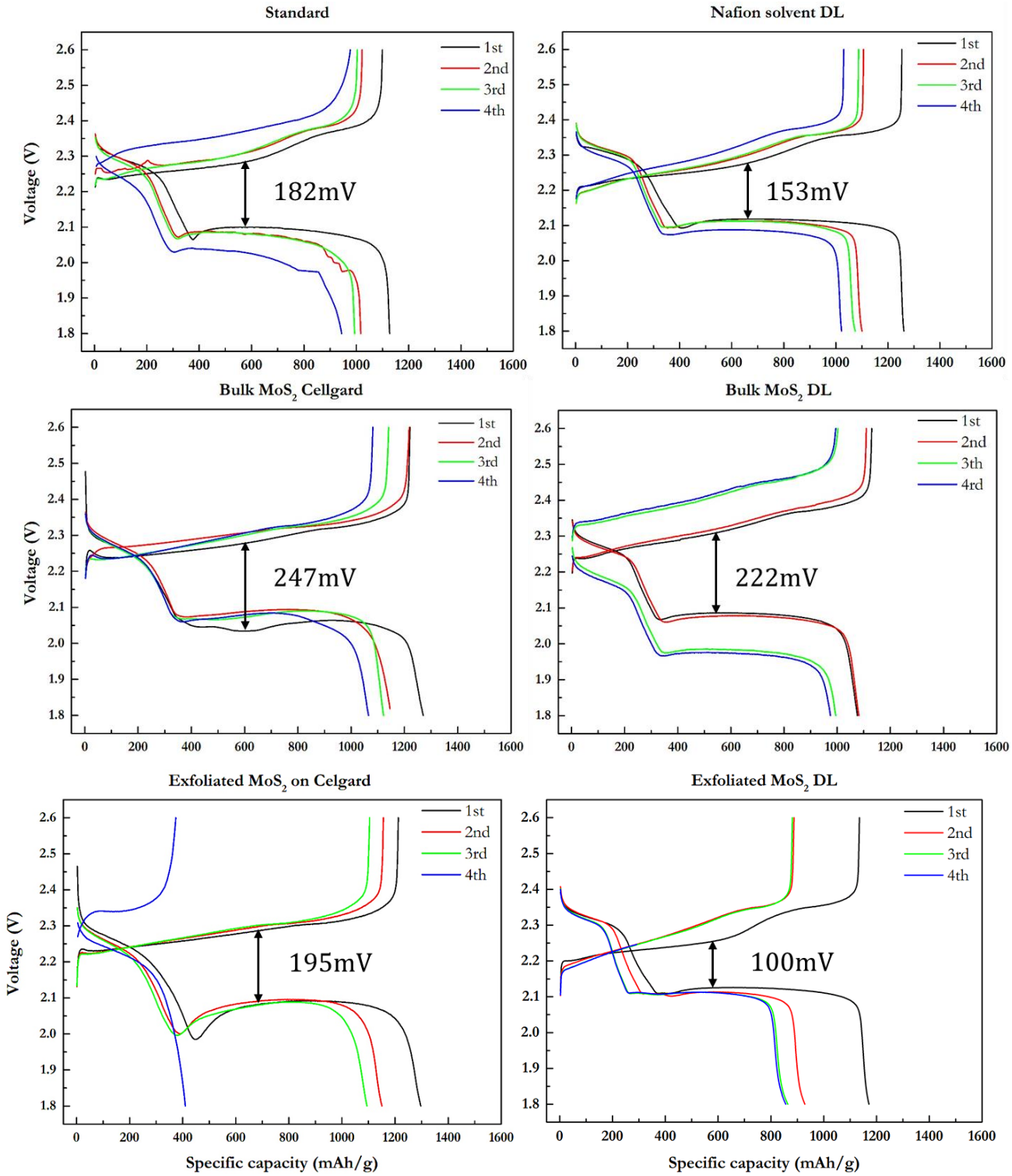

Figure 3-14 galvanometric capacity graphic performed on standard sulfur battery, on nafion solvent double layer, on bulk and exfoliated MoS2 interlayers placed on double layer and on celgard at C/10

3.2.3.2 C/5

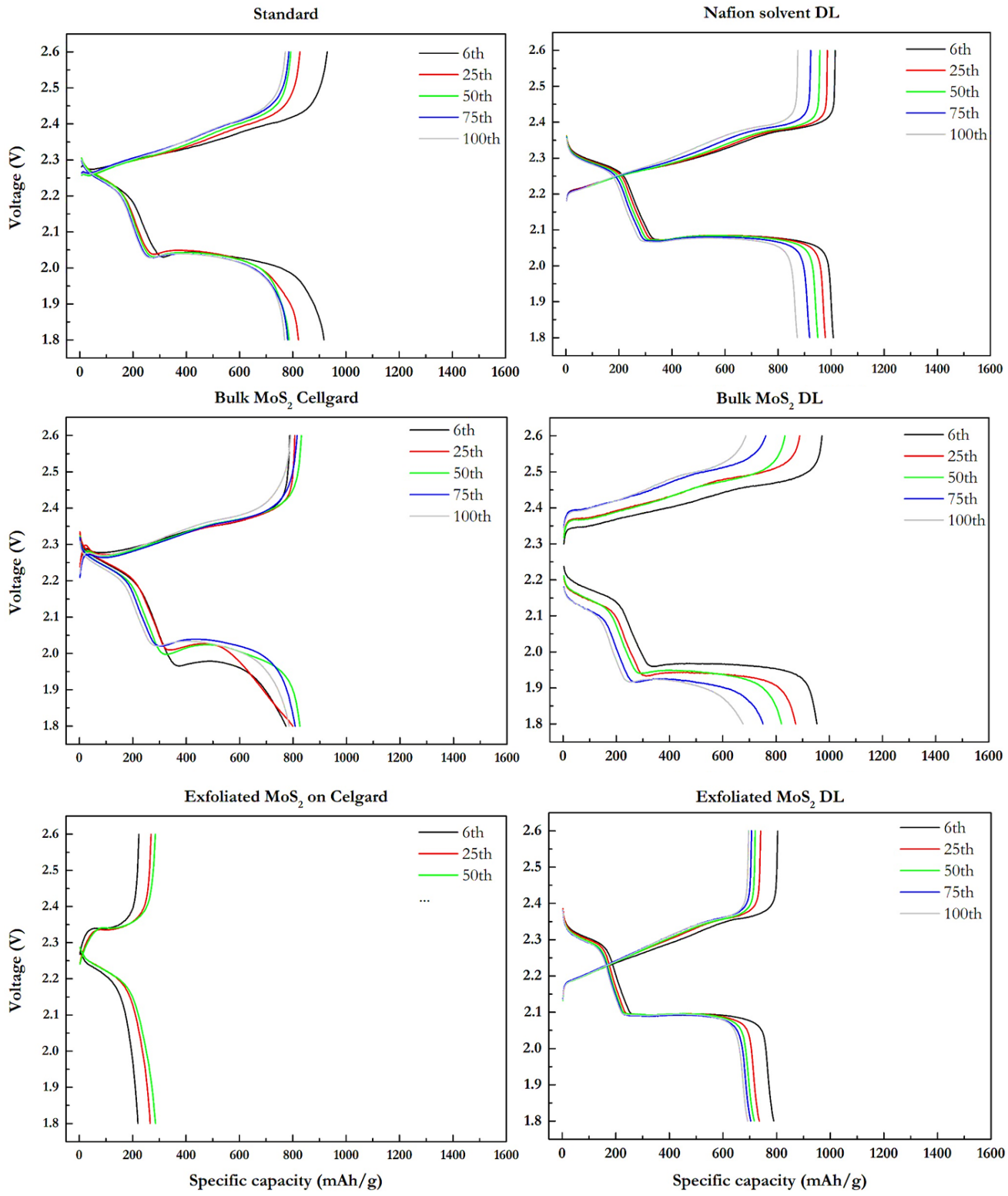

Figure 3-15 galvanometric capacity graphic performed on standard sulfur battery, on nafion solvent double layer, on bulk and exfoliated MoS2 interlayers placed on double layer and on celgard at C/5

Figure 3.15 reveals C/5 galvanometric capacity graphs of sulfur batteries with different designs, is observed the discharging of the batteries until the 100th cycle when the test was

terminated, where is possible to witness a reduction of EOD in the 6th cycle compared with 5th in C/10 cycles. This is transversal to all tested cells and is a consequence of increasing C-rate.

Standard sulfur discharge capacity drops from 54% to 46% for the 6th and 100th cycles respectively, revealing an 8% loss in sulfur utilization during this cycling period.

Nafion solvent DL presents very flat and long discharge capacity lines that result from transformation of long chain PS into short chain ones. After one hundred cycles efficiency dropped from initial 60% (6th cycle) to 52% representing 8 percentage points loss of sulfur utilization. This means the DL is performing a good job on PS blocking throughout cycling, a result of efficient kinetics reactions and improved physical PS trapping. Bulk MoS_2 DL drop from 56% (6th cycle) to a low 40% which is a considerable decrease by cycle. One possible explanation is the shuttling effect and higher amount of soluble PS in the electrolyte. In addition, (ΔE) also increases by each cycle, meaning a decrease in cell kinetics, resulting from an increase in viscosity confirming that PS are present in the electrolyte. For exfoliated samples DL discharge values drop from 47% (6th cycle) to 41%. Even though values are lower than the standard sulfur test cells the difference between 6th and 100th cycle is lower, meaning a good structural stability of the DL and a good polysulfide blocking along cycling.

Celgard separator coated by bulk shows short discharge capacity values, meaning sulfur utilization is not as high. Although amount of sulfur used was not as high, the ability to maintain its amount for each cycle revealed to be very good, showing the same amount of sulfur being used in 6th and 100th cycle. This means that interlayer formed kept its structural integrity during battery charge and discharge, keeping its function to block PS shuttle for a long time.

Celgard separator coated by exfoliated MoS_2 shows a short cell life, coupled with very low EOD values, perhaps a result of excessive deposition of resistive Li_2S2/Li_2S PS on top of MoS_2 coating preventing the passage of ions and PS to the cathode and reducing the amount of sulfur interaction [5], [17], [22].

3.2.4 Coulombic efficiency

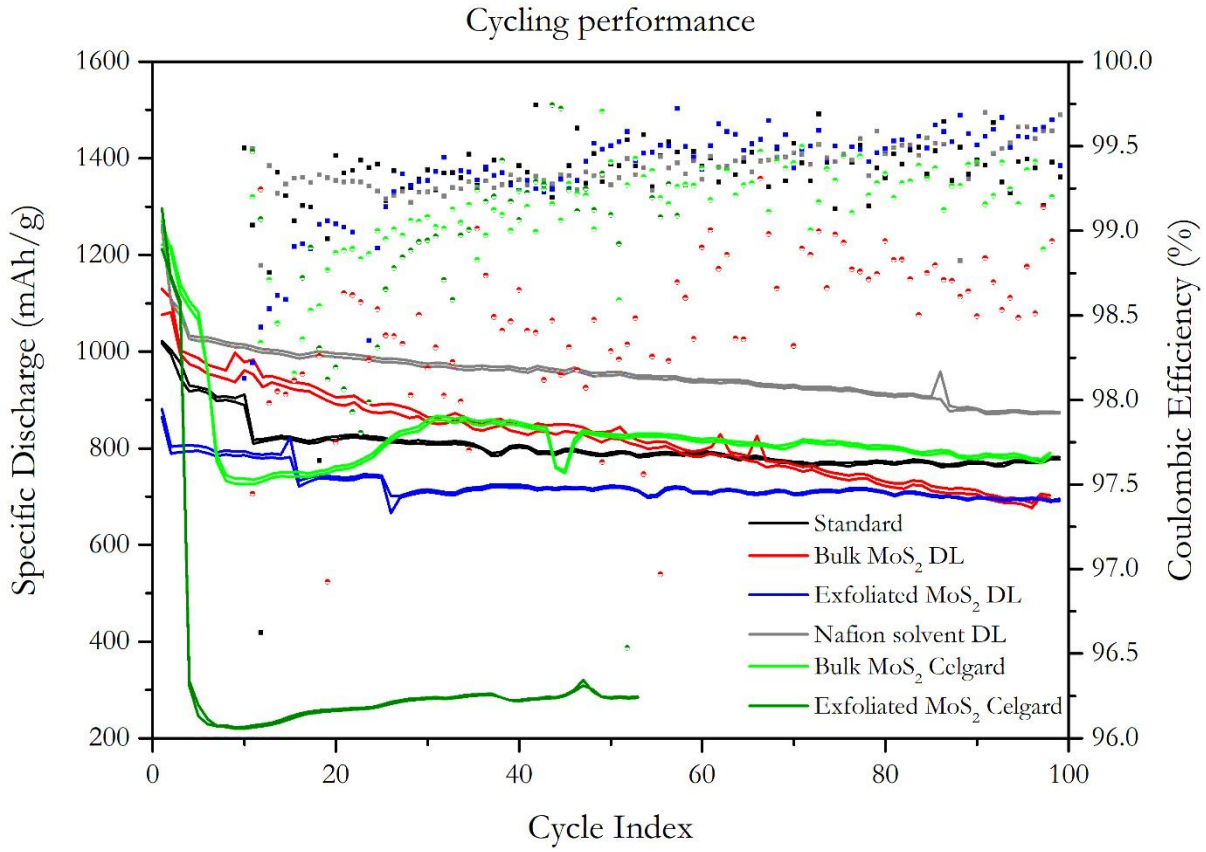

Figure 3-16 Coulombic efficiencies and capacity performance during cycling for standard sulfur batteries, bulk MoS_2 DL, Exfoliated MoS_2 DL, bulk MoS_2 separator, exfoliated MoS_2 separator a nafion solvent DL

Figure 3.16 reveals that standard sulfur cathode keeps an impressive 99.3% coulombic efficiency for the 100th cycle, this reveals good ability to prevent polysulfide shuttle during cycling.

All types of test cells showed Coulombic efficiencies above 98% by the 100th cycle bulk DL at 98.8%, bulk MoS_2 on celgard with 99.2% performing just below standard sulfur batteries, exfoliated DL at 99.4% and at the top of coulombic efficiency performance with impressive 99.7% nafion solvent DL. This suggests a reliable stability for the one hundred cycles, demonstrating the efficiency of the second layer on top of the cathode and that stability of this second layer is increased when we use a different solvent on the second layer. In this test exfoliated MoS_2 on Celgard test cell was excluded because it couldn't reach the one hundred cycles requirement for this test.

For discharge capacity the fade per cycle was studied in order to understand the battery performance during the 100 cycles. The standard battery shows a capacity fade of 0.08% per cycle, the same found in nafion solvent DL. The amount of sulfur lost per cycle is the same in both of these configurations, possibly due to same capability to block PS. However initial sulfur utilization is higher on nafion DL (demonstrated in figure 3.16), possibly due to less resistive PS

coating on the DL. Therefore, the 100th cycle of nafion presents higher discharge values than standard sulfur cells. For the exfoliated DL, loss decreases 0.06% per cycle, meaning that this material is more stable during cycling and efficiently trapping PS.

For bulk MoS_2 on Celgard the capacity fades initially but then increase. This effect can be observed on both of Celgard double layers, and it is possibly related to the growth of a resistive PS layer on top of the separator coating [4], [5], [10], [17], [22].

4 Conclusions

Exfoliated thin flakes of 2H MoS_2, were developed and used as the interlayer's active material, to trap PS in the cathode of Li-S test cells. Afore mentioned, the exfoliation was performed through solvothermal lithium intercalation of MoS_2 bulk structure and proceeded by water sonication, to promote layer separation. Therefore, resulting in thin MoS_2 flakes with increased surface area and enhanced electronic properties, features favorable for improved trapping of PS.

Through exfoliation, the number of layers of 2H MoS_2 flakes decreased considerably and the flake's length reduced up to 56 times. Moreover, using XRD was calculated the MoS_2 lattice parameters and interplanar distance which revealed an increase of interplanar distance, consistent with lithium insertion. Followed by a consequential decrease after sonication. Furthermore, the presence of thinner layers was demonstrated in Raman by the redshift of A_1g peak and SEM image analysis. In addition, optical spectroscopy showed effects of quantum confinement, with A and B exitonic peaks appearing in exfoliated samples. The 3h synthesis sonicated for 10h demonstrated, to be the least time-consuming among successful lithium intercalation methods, so was therefore chosen to produce in larger quantities, to be used as the interlayer's active material.

Electrochemical characterization, of distinct Li-S test cells (each with different interlayers), was explored, and compared to a standardized Li-S test cell. The purpose of this comparison was to understand the effects of the different interlayers in the standard battery. Afore mentioned, interlayers were spread either on to the cathode (DL), or the separator, to test the effects of the interlayer position. Furthermore, carbon black, bulk and exfoliated MoS_2, were compared as active materials of the interlayers.

The study of the position of the interlayer revealed higher initial sulfur capacity when placing the interlayer on celgard. However, after the first cycle, the sulfur utilization decayed faster and kinetics were slower for this type of interlayer configuration, suggesting a resistive PS passivation of the interlayer placed on the separator.

Between the different active materials, the CB DL presented a 9 point percentile increase of sulfur utilization in the first cycle. With a decay of 0.08 percental points of the initial sulfur utilization per cycle, the same degradation per cycle observed for standard sulfur. In addition, coulombic efficiency was very high, determined at 99.7% for the 100^{th} cycle, meaning the interlayer has high stability in cycling and high sulfur utilization. Nonetheless, ΔE had a 16 percental points improvement, representing better kinetics than standard sulfur, a result of low amount of PS dissolved in the electrolyte.

On another hand, when using exfoliated MoS_2 as the active material for the DL, can be observed a 4 point percentile increase in sulfur discharge capacity for the first cycle, linked with higher sulfur utilization. Furthermore, an impressively low capacity fade of 0.06% per cycle, means less amount of sulfur being loss to PS shuttling. Coulombic efficiency was determined at 99.4%, a result of high stability in cycling and high sulfur utilization. Moreover, ΔE had a 45% decrease, related with improved kinetics of the test cell, meaning PS are not dissolving into the electrolyte, therefore improving conductivity. Nyquist plots also revealed less resistivity in the solvent at just 3Ω, so the results show the exfoliated MoS_2 interlayer has good ionic transport paths, and improved PS capture.

4.1 Future perspectives

For near future work, lithium intercalation method could change from solvothermal to electrochemical lithium intercalation, to achieve a more controlled lithium insertion. In addition, the method to extract MoS_2 from liquid could be improved using freeze drying to reduce loss nanostructured flakes. Moreover, characterization techniques like XPS and AFM can be used to understand the effects of band gap change, and the number of layers in the flakes, respectively.

On the other hand, MoS_2 could be incorporated in the electrolyte or inserted into a polymeric conductive matrix to further understand the effects of the material on PS trapping. Nevertheless, the use nafion as a solvent for the MoS_2 DL, could be further explored to prevent the use of the same solvent for both cathode and DL, therefore reducing the risk of mixing the different.

5 References:

[1] D. Bresser, S. Passerini, and B. Scrosati, "Recent progress and remaining challenges in sulfur-based lithium secondary batteries - a review," *Chem. Commun.*, vol. 49, no. 90, pp. 10545–10562, 2013, doi: 10.1039/c3cc46131a.

[2] B. Jin, J. Kim, and H. Gu, "Electrochemical properties of lithium – sulfur batteries," vol. 117, pp. 148–152, 2003, doi: 10.1016/S0378-7753(03)00113-7.

[3] V. Etacheri, R. Marom, R. Elazari, G. Salitra, and D. Aurbach, "Challenges in the development of advanced Li-ion batteries: A review," *Energy Environ. Sci.*, vol. 4, no. 9, pp. 3243–3262, 2011, doi: 10.1039/c1ee01598b.

[4] A. Manthiram, Y. Fu, S. Chung, C. Zu, and Y. Su, "Rechargeable Lithium − Sulfur Batteries," 2014.

[5] L. Tan, X. Li, Z. Wang, H. Guo, and J. Wang, "Lightweight Reduced Graphene

Oxide@MoS2 Interlayer as Polysulfide Barrier for High-Performance Lithium-Sulfur Batteries," *ACS Appl. Mater. Interfaces*, vol. 10, no. 4, pp. 3707–3713, 2018, doi: 10.1021/acsami.7b18645.

[6] A. N. Mistry and P. P. Mukherjee, "'Shuttle' in Polysulfide Shuttle: Friend or Foe?," *J. Phys. Chem. C*, vol. 122, no. 42, pp. 23845–23851, 2018, doi: 10.1021/acs.jpcc.8b06077.

[7] W. Kang *et al.*, "A review of recent developments in rechargeable lithium-sulfur batteries," *Nanoscale*, vol. 8, no. 37, pp. 16541–16588, 2016, doi: 10.1039/c6nr04923k.

[8] B. Jin, J. U. Kim, and H. B. Gu, "Electrochemical properties of lithium-sulfur batteries," *J. Power Sources*, vol. 117, no. 1–2, pp. 148–152, 2003, doi: 10.1016/S0378-7753(03)00113-7.

[9] H. Lin *et al.*, "Electrocatalysis of polysulfide conversion by sulfur-deficient MoS2 nanoflakes for lithium-sulfur batteries," *Energy Environ. Sci.*, vol. 10, no. 6, pp. 1476–1486, 2017, doi: 10.1039/c7ee01047h.

[10] N. Jayaprakash, J. Shen, S. S. Moganty, A. Corona, and L. A. Archer, "Porous hollow carbon@sulfur composites for high-power lithium-sulfur batteries," *Angew. Chemie - Int. Ed.*, vol. 50, no. 26, pp. 5904–5908, 2011, doi: 10.1002/anie.201100637.

[11] X. B. Cheng, R. Zhang, C. Z. Zhao, and Q. Zhang, "Toward Safe Lithium Metal Anode in Rechargeable Batteries: A Review," *Chem. Rev.*, vol. 117, no. 15, pp. 10403–10473, 2017, doi: 10.1021/acs.chemrev.7b00115.

[12] V. S. Kolosnitsyn and E. V. Karaseva, "Lithium-sulfur batteries: Problems and solutions," *Russ. J. Electrochem.*, vol. 44, no. 5, pp. 506–509, 2008, doi: 10.1134/S1023193508050029.

[13] L. Chen and L. L. Shaw, "Recent advances in lithium e sulfur batteries," *J. Power Sources*, vol. 267, pp. 770–783, 2014, doi: 10.1016/j.jpowsour.2014.05.111.

[14] Y. V. Mikhaylik and J. R. Akridge, "Polysulfide shuttle study in the Li/S battery system," *J. Electrochem. Soc.*, vol. 151, no. 11, pp. 1969–1976, 2004, doi: 10.1149/1.1806394.

[15] J. Yan, X. Liu, and B. Li, "Capacity Fade Analysis of Sulfur Cathodes in Lithium – Sulfur Batteries," 2016, doi: 10.1002/advs.201600101.

[16] X. Xie, Z. Ao, D. Su, J. Zhang, and G. Wang, "MoS2/graphene composite anodes with enhanced performance for sodium-ion batteries: The role of the two-dimensional heterointerface," *Adv. Funct. Mater.*, vol. 25, no. 9, pp. 1393–1403, 2015, doi: 10.1002/adfm.201404078.

[17] Z. A. Ghazi *et al.*, "MoS2/Celgard Separator as Efficient Polysulfide Barrier for Long-Life Lithium–Sulfur Batteries," *Adv. Mater.*, vol. 29, no. 21, pp. 1–6, 2017, doi: 10.1002/adma.201606817.

[18] A. Hayashi, T. Ohtomo, F. Mizuno, K. Tadanaga, and M. Tatsumisago, "All-solid-state Li/S batteries with highly conductive glass-ceramic electrolytes," *Electrochem. commun.*, vol. 5, no. 8, pp. 701–705, 2003, doi: 10.1016/S1388-2481(03)00167-X.

[19] S. H. Kim, J. H. Kim, S. J. Cho, and S. Y. Lee, "All-Solid-State Printed Bipolar Li–S Batteries," *Adv. Energy Mater.*, vol. 9, no. 40, pp. 1–10, 2019, doi: 10.1002/aenm.201901841.

[20] M. Wang *et al.*, "A multi-core-shell structured composite cathode material with a conductive polymer network for Li-S batteries," *Chem. Commun.*, vol. 49, no. 87, pp. 10263–10265, 2013, doi: 10.1039/c3cc45412f.

[21] Y. Xia *et al.*, "A poly (vinylidene fluoride-hexafluoropropylene) based three-dimensional network gel polymer electrolyte for solid-state lithium-sulfur batteries," *Chem. Eng. J.*, vol. 358, pp. 1047–1053, 2019, doi: 10.1016/j.cej.2018.10.092.

[22] S. Yang, J. Zhang, T. Tan, Y. Zhao, N. Liu, and H. Li, "A 3D MoS2/graphene microsphere coated separator for excellent performance Li-S batteries," *Materials (Basel).*, vol. 11, no. 10, pp. 1–13, 2018, doi: 10.3390/ma11102064.

[23] Y. You *et al.*, "Three-dimensional MoS2/rGO foams as efficient sulfur hosts for high-performance lithium-sulfur batteries," *Chem. Eng. J.*, vol. 355, pp. 671–678, 2019, doi: 10.1016/j.cej.2018.08.176.

[24] B. Yu *et al.*, "1T-MoS2 nanotubes wrapped with N-doped graphene as highly-efficient absorbent and electrocatalyst for Li–S batteries," *J. Power Sources*, vol. 447, no. October 2019, 2020, doi: 10.1016/j.jpowsour.2019.227364.

[25] S. Bag, C. Zhou, P. J. Kim, V. G. Pol, and V. Thangadurai, "LiF modified stable flexible PVDF-garnet hybrid electrolyte for high performance all-solid-state Li–S batteries," *Energy Storage Mater.*, vol. 24, no. August, pp. 198–207, 2020, doi: 10.1016/j.ensm.2019.08.019.

[26] P. Guo, D. Liu, Z. Liu, X. Shang, Q. Liu, and D. He, "Dual functional MoS2/graphene interlayer as an efficient polysulfide barrier for advanced lithium-sulfur batteries," *Electrochim. Acta*, vol. 256, pp. 28–36, 2017, doi: 10.1016/j.electacta.2017.10.003.

[27] A. Fernicola, F. Croce, B. Scrosati, T. Watanabe, and H. Ohno, "LiTFSI-BEPyTFSI as an improved ionic liquid electrolyte for rechargeable lithium batteries," *J. Power Sources*, vol. 174, no. 1, pp. 342–348, 2007, doi: 10.1016/j.jpowsour.2007.09.013.

[28] L. Edman, M. M. Doeff, A. Ferry, J. Kerr, and L. C. De Jonghe, "Transport properties of the solid polymer electrolyte system P(EO)nLiTFSI," *J. Phys. Chem. B*, vol. 104, no. 15, pp. 3476–3480, 2000, doi: 10.1021/jp993897z.

[29] J. Wang, K. Xie, and B. Wei, "Advanced engineering of nanostructured carbons for lithium – sulfur batteries," *Nano Energy*, 2015, doi: 10.1016/j.nanoen.2015.05.006.

[30] R. Wang *et al.*, "Effect of Different Binders on the Electrochemical Performance of Metal Oxide Anode for Lithium-Ion Batteries," *Nanoscale Res. Lett.*, vol. 12, 2017, doi: 10.1186/s11671-017-2348-6.

[31] H. Althues, S. Dörfler, S. Thieme, P. Strubel, and S. Kaskel, "Sulfur Cathodes 2 . 1 Cathode Design Criteria," 2019.

[32] G. Deokar, D. Vignaud, R. Arenal, P. Louette, and J. Colomer, "Synthesis and characterization of MoS 2 nanosheets," vol. 075604.

[33] J. N. Coleman *et al.*, "Two-dimensional nanosheets produced by liquid exfoliation of layered materials," *Science (80-.).*, vol. 331, no. 6017, pp. 568–571, 2011, doi: 10.1126/science.1194975.

[34] M. Chhowalla, H. S. Shin, G. Eda, L. J. Li, K. P. Loh, and H. Zhang, "The chemistry of two-dimensional layered transition metal dichalcogenide nanosheets," *Nat. Chem.*, vol. 5, no. 4, pp. 263–275, 2013, doi: 10.1038/nchem.1589.

[35] G. Eda, T. Fujita, H. Yamaguchi, D. Voiry, M. Chen, and M. Chhowalla, "Coherent atomic and electronic heterostructures of single-layer MoS 2," *ACS Nano*, vol. 6, no. 8, pp. 7311–7317, 2012, doi: 10.1021/nn302422x.

[36] H. Ma, Z. Shen, and S. Ben, "Understanding the exfoliation and dispersion of MoS2 nanosheets in pure water," *J. Colloid Interface Sci.*, vol. 517, no. November, pp. 204–212, 2018, doi: 10.1016/j.jcis.2017.11.013.

[37] J. Xia *et al.*, "Phase evolution of lithium intercalation dynamics in 2H-MoS 2," *Nanoscale*, vol. 9, no. 22, pp. 7533–7540, 2017, doi: 10.1039/c7nr02028g.

[38] W. Choi, N. Choudhary, G. H. Han, J. Park, D. Akinwande, and Y. H. Lee, "Recent development of two-dimensional transition metal dichalcogenides and their applications," *Mater. Today*, vol. 20, no. 3, pp. 116–130, 2017, doi: 10.1016/j.mattod.2016.10.002.

[39] D. Wang, F. Wu, Y. Song, C. Li, and L. Zhou, "Large-scale production of defect-free MoS2 nanosheets via pyrene-assisted liquid exfoliation," *J. Alloys Compd.*, vol. 728, pp. 1030–1036, 2017, doi: 10.1016/j.jallcom.2017.09.074.

[40] S. Nos, P. Joensen, R. F. Frindt, and S. R. Morrison, "0025-5408 / 86 $ 3 . 00 + . 00 C o p y r i g h t (c) 1986 P e r g a m o n P r e s s L t d . (Received January by A . Wold)," vol. 21, no. c, pp. 457–461, 1986.

[41] D. Xuan, Y. Zhou, W. Nie, and P. Chen, "Sodium alginate-assisted exfoliation of MoS2 and its reinforcement in polymer nanocomposites," *Carbohydr. Polym.*, vol. 155, pp. 40–48,

2017, doi: 10.1016/j.carbpol.2016.08.052.

[42] L. Wang, Z. Xu, W. Wang, and X. Bai, "Atomic mechanism of dynamic electrochemical lithiation processes of MoS2 nanosheets," *J. Am. Chem. Soc.*, vol. 136, no. 18, pp. 6693–6697, 2014, doi: 10.1021/ja501686w.

[43] A. Splendiani *et al.*, "Emerging photoluminescence in monolayer MoS 2," *Nano Lett.*, vol. 10, no. 4, pp. 1271–1275, 2010, doi: 10.1021/nl903868w.

[44] M. A. Py and R. R. Haering, "STRUCTURAL DESTABILIZATION INDUCED BY LITHIUM INTERCALATION IN MoS2 AND RELATED COMPOUNDS.," *Can. J. Phys.*, vol. 61, no. 1, pp. 76–84, 1983, doi: 10.1139/p83-013.

[45] J. Xia *et al.*, "Phase evolution of lithium intercalation dynamics in 2H-MoS 2," *Nanoscale*, vol. 9, no. 22, pp. 7533–7540, 2017, doi: 10.1039/c7nr02028g.

[46] Y. D. Liu *et al.*, "Preparation, characterization and photoelectrochemical property of ultrathin MoS2 nanosheets via hydrothermal intercalation and exfoliation route," *J. Alloys Compd.*, vol. 571, pp. 37–42, 2013, doi: 10.1016/j.jallcom.2013.03.031.

[47] A. Review, "Conventional and Microwave Hydrothermal Synthesis and Application of Functional Materials : A Review," 2019, doi: 10.3390/ma12071177.

[48] E. Giovanelli, A. Castellanos-gomez, and E. M. Pérez, "Surfactant-Free Polar-to-Non-Polar-Phase Transfer of Exfoliated MoS 2 Two-Dimensional Colloids," pp. 8–11.

[49] Y. Peng *et al.*, "Hydrothermal synthesis of MoS 2 and its pressure-related crystallization," *J. Solid State Chem.*, vol. 159, no. 1, pp. 170–173, 2001, doi: 10.1006/jssc.2001.9146.

[50] Z. Xia, Y. Tao, Z. Pan, and X. Shen, "Enhanced photocatalytic performance and stability of 1T MoS 2 transformed from 2H MoS 2 via Li intercalation," *Results Phys.*, vol. 12, pp. 2218–2224, 2019, doi: 10.1016/j.rinp.2019.01.020.

[51] C. CULLITY, B. D.; MORRIS, *ELEMENTS OF X-RAY DIFFRACTION*. .

[52] V. An and Y. Irtegov, "Tribological properties of nanolamellar MoS2 doped with copper nanoparticles," *J. Nanomater.*, vol. 2014, no. September 2014, 2014, doi: 10.1155/2014/731073.

[53] P. Electronics, "Ac ce explained in terms of surface energies of substrates and classical theory of nucleation and d M us pt," 2018.

[54] C. P. Veeramalai, F. Li, Y. Liu, Z. Xu, T. Guo, and T. W. Kim, "Enhanced field emission properties of molybdenum disulphide few layer nanosheets synthesized by hydrothermal method," *Appl. Surf. Sci.*, vol. 389, no. October, pp. 1017–1022, 2016, doi: 10.1016/j.apsusc.2016.08.031.

[55] C. Innovation, N. Zealand, S. Synchrotron, and R. Lightsource, *X-ray diffraction for*

characterizing metallic films 1. 2014.

[56] X. Zhang, X. Qiao, W. Shi, J. Wu, D. Jiang, and P. Tan, "Chem Soc Rev transition metal dichalcogenides from monolayer ," *Chem. Soc. Rev.*, 2015, doi: 10.1039/c4cs00282b.

[57] P. R. Wu, W. Li, Y. M. Feng, T. Ge, Z. Liu, and Z. L. Cheng, "Fabrication and tribological properties of oil- soluble MoS2 nanosheets decorated by oleic diethanolamide borate," *J. Alloys Compd.*, vol. 770, pp. 441–450, 2019, doi: 10.1016/j.jallcom.2018.08.156.

[58] N. M. O, "Electrochemically Reversible Sodium Intercalation of Layered," vol. 16, no. 42, pp. 43–55, 2009.

[59] "Raman spectroscopy explained Raman spectroscopy explained," no. September, pp. 1–48, 2018.

[60] L. Wirtz, "Phonons in single-layer and few-layer MoS 2 and WS 2," vol. 155413, pp. 1–8, 2011, doi: 10.1103/PhysRevB.84.155413.

[61] B. Chakraborty, H. S. S. R. Matte, A. K. Sood, and C. N. R. Rao, "Layer-dependent resonant Raman scattering of a few layer MoS 2," no. June 2012, pp. 92–96, 2013, doi: 10.1002/jrs.4147.

[62] F. Mos *et al.*, "Anomalous Lattice Vibrations of Single-," vol. 4, no. 5, pp. 2695–2700, 2010.

[63] A. Thin, "Evolution of Electronic Structure in," no. Xx, 2012.

[64] Y. Cheng, Z. Zhu, and U. Schwingenschlo, "RSC Advances Role of interlayer coupling in ultra thin MoS 2," pp. 7798–7802, 2012, doi: 10.1039/c2ra20132a.

[65] R. Gillen and J. Maultzsch, "Light-Matter Interactions in Two-Dimensional Transition Metal Dichalcogenides: Dominant Excitonic Transitions in Mono- and Few-Layer MoX-2 and Band Nesting," *IEEE J. Sel. Top. Quantum Electron.*, vol. 23, no. 1, pp. 1–12, 2017, doi: 10.1109/JSTQE.2016.2604359.

[66] O. T, Mai T. Bernard, Tribolle.Vincent Vivier.Mark E., "On the Impedance Response of Reactions Influenced by Mass Transfer," *Russ. J. Electrochem.*, vol. 53, no. 9, pp. 932–940, 2017, doi: 10.1134/S1023193517090142.

[67] Z. A. Ghazi *et al.*, "MoS2/Celgard Separator as Efficient Polysulfide Barrier for Long-Life Lithium–Sulfur Batteries," *Adv. Mater.*, vol. 29, no. 21, 2017, doi: 10.1002/adma.201606817.

[68] A. Huiling, A. Bonanni, Z. Sofer, and M. Pumera, "Electrochemistry Communications An electrochemical impedance spectroscopic investigation," vol. 50, pp. 39–42, 2015, doi: 10.1016/j.elecom.2014.10.018.

[69] T. S. Mathis, N. Kurra, X. Wang, D. Pinto, and P. Simon, "Energy Storage Data

Reporting in Perspective — Guidelines for Interpreting the Performance of Electrochemical Energy Storage Systems," vol. 1902007, pp. 1–13, 2019, doi: 10.1002/aenm.201902007.

[70] D. Dragu, M. Buda, and T. V. I. Ş. An, "CYCLIC VOLTAMMETRY SIMULATION USING ORTHOGONAL COLLOCATION : COMPARISON WITH EXPERIMENTAL DATA AND MEASURING THE ELECTROCHEMICAL RATE CONSTANT," vol. 71, 2009.

[71] K. J. Rountree, B. D. Mccarthy, E. S. Rountree, T. T. Eisenhart, and J. L. Dempsey, "A Practical Beginner ' s Guide to Cyclic Voltammetry," 2017, doi: 10.1021/acs.jchemed.7b00361.

[72] L. Tan, X. Li, Z. Wang, H. Guo, and J. Wang, "Lightweight Reduced Graphene Oxide @ MoS 2 Interlayer as Polysul fi de Barrier for High-Performance Lithium − Sulfur Batteries," 2018, doi: 10.1021/acsami.7b18645.